

TOWARDS OPTIMAL STEADY STATE CONTROL OF MULTI-TERMINAL HVDC  
SYSTEMS

by

Youssef Al Falah

A thesis submitted in conformity with the requirements  
for the degree of Master of Applied Science - M.A.Sc  
Edward S. Rogers Department of Electrical and Computer Engineering  
University of Toronto

© Copyright 2022 by Youssef Al Falah

# Towards Optimal Steady State Control of Multi-terminal HVDC Systems

Youssef Al Falah

Master of Applied Science - M.A.Sc

Edward S. Rogers Department of Electrical and Computer Engineering

University of Toronto

2022

## **Abstract**

This thesis applies linear-convex optimal steady state (LC-OSS) control to a multi-terminal high voltage DC (MTDC) system connecting AC systems. LC-OSS control framework uses real-time feedback to regulate the output of an LTI system to the solution of a constrained convex optimization problem. We first show that the LC-OSS control framework recovers some of the existing MTDC controllers in the literature. Then, we propose a dynamic controller which drives the AC systems to collectively respond to power load variation while minimizing DC losses and maintaining DC line currents within acceptable limits. Finally, we evaluate the controller's performance in simulation and verify that it is able to drive an MTDC test system to a desired optimal operating point.

## Acknowledgments

First and foremost, all praises and thanks are due to God, the Almighty, for granting me all what it takes to accomplish this thesis. The countless blessings that He has bestowed upon me are beyond what I deserve.

I would like to acknowledge my supervisors Professor Josh Taylor and Professor John Simpson-Porco. Their enthusiasm and diligence were my source of motivation and inspiration that fostered my learning and research skills during my time at the University of Toronto. I would not have been able to make it without their invaluable guidance at every milestone of my M.A.Sc journey. I thank you for your patience and support.

I would also like to acknowledge my thesis committee members, Professor Lacra Pavel and Professor Peter Lehn. I thank you for granting me the opportunity to learn from your constructive feedback.

I thank my friends for their support and encouragement throughout this journey. I name of them, Ahmad Sibahi, whom I was first introduced to the new lifestyle in Canada with. I thank you for making this a smooth transition.

Finally I would like to thank my family. To my parents, Mounir and Maha, I owe you everything I have become. I thank you for your unconditional care, love, and support. Making you proud has always been a pivotal motivation for me to keep going. Thank you.

Last but not least, I thank my loving wife, Youmna, for being the best and most supportive and understanding partner anyone could ask for. No words can describe my appreciation to the sacrifice that you have made to make this journey a success in all aspects. I will forever be grateful to have you by my side.

# Contents

<b>List of Figures</b>	<b>vi</b>
<b>List of Tables</b>	<b>vii</b>
<b>List of Symbols</b>	<b>viii</b>
<b>1 Introduction</b>	<b>1</b>
1.1 Motivation . . . . .	1
1.2 Literature Review . . . . .	2
1.3 Contributions . . . . .	4
1.4 Thesis Layout . . . . .	4
<b>2 Optimization and Control Background</b>	<b>6</b>
2.1 Convex Optimization . . . . .	6
2.1.1 Optimization Problems . . . . .	6
2.1.2 Convexity (Sets, Functions, and Optimization) . . . . .	7
2.1.3 The Karush-Kuhn-Tucker Conditions . . . . .	8
2.2 Linear-Convex Optimal Steady-State Control . . . . .	9
2.3 Mathematical and Control Theory Tools . . . . .	12
<b>3 MTDC System Modeling</b>	<b>15</b>
3.1 Network Topology . . . . .	15
3.2 HVDC System Model . . . . .	17
3.2.1 Modeling of a Single HVDC System $l$ . . . . .	17
3.2.2 Modeling of the Set of $M$ HVDC Systems . . . . .	23
3.3 AC System Model . . . . .	23
3.3.1 Modeling of a Single AC System $h$ . . . . .	23
3.3.2 Modeling of the Set of $N$ AC Systems . . . . .	26
3.4 Overall System Model . . . . .	27
<b>4 OSS Control in MTDC Systems</b>	<b>28</b>
4.1 Special Cases of LC-OSS Control in the Literature . . . . .	28
4.1.1 Distributed Power Consensus Control . . . . .	29

4.1.2	Decentralized Voltage Control . . . . .	33
4.2	OSS Problem Formulation . . . . .	37
4.3	LC-OSS HVDC Controller . . . . .	40
4.4	Stability Analysis of the Proposed Controller . . . . .	42
<b>5</b>	<b>Simulation Results</b>	<b>47</b>
5.1	Test System . . . . .	47
5.1.1	HVDC Test Systems Parameters . . . . .	49
5.1.2	AC Test Systems Parameters . . . . .	50
5.2	Cost Function Parameters . . . . .	51
5.3	Results . . . . .	52
<b>6</b>	<b>Conclusion and Future Work</b>	<b>60</b>
6.1	Conclusion . . . . .	60
6.2	Future Work . . . . .	60
<b>A</b>	<b>Chapter 3 Supplements</b>	<b>62</b>
A.1	Linearization of the AC System Model . . . . .	62
<b>B</b>	<b>Chapter 4 Supplements</b>	<b>64</b>
B.1	Derivation of the expression of $\tilde{G}_\eta(0)$ . . . . .	64
B.2	System Steady State Derivation . . . . .	65
	<b>Bibliography</b>	<b>67</b>

# List of Figures

2.1	Block diagram of general OSS control architecture . . . . .	12
3.1	Network topology of the MTDC system . . . . .	16
3.2	Circuit diagram of HVDC system $l$ . . . . .	18
3.3	Equivalent circuit diagram of HVDC system $l$ . . . . .	19
4.1	Block diagram of the MTDC-OSS controller . . . . .	43
4.2	Block diagram of inner loop . . . . .	44
5.1	Topology of the Overall Test System . . . . .	48
5.2	Topology of HVDC test systems . . . . .	50
5.3	$\Delta f$ of AC Systems . . . . .	53
5.5	$\Delta P_{\text{vsc}}$ of the HVDC systems . . . . .	54
5.7	Adjusted power load disturbance in AC systems . . . . .	55
5.9	$\Delta P_{\text{m}}$ of AC Systems . . . . .	56
5.11	$\Delta P_{\text{loss}}$ of HVDC systems 1 and 2 . . . . .	57
5.13	$i_{\text{L},1}$ of HVDC system 1 . . . . .	58
5.15	$i_{\text{L},2}$ of HVDC system 2 . . . . .	59
B.1	Block diagram of the system (4.7)-(4.8) . . . . .	64

# List of Tables

5.1	Scheduled power transfer between AC systems . . . . .	48
5.2	Operating point bus voltage in HVDC test systems . . . . .	49
5.3	Operating point link currents of HVDC test systems . . . . .	49
5.4	Operating point power injected into the HVDC test systems at each bus	49
5.5	Grid line parameters of HVDC test systems . . . . .	50
5.6	Grid line lengths of HVDC test systems . . . . .	50
5.7	Parameters of AC test systems . . . . .	51
5.8	Operating point values of AC test systems . . . . .	51
5.9	Parameters of cost functions $f_1(y)$ , $f_2(y)$ , and $f_3(y)$ . . . . .	52
5.10	AC systems' load power disturbance . . . . .	52

# List of Symbols

$\mathbb{1}_n, \mathbb{1}_{m \times n}$	The $n \times 1$ vector and $m \times n$ matrix of all ones; subscript is omitted when it is clear from context.
$\mathbb{0}_n, \mathbb{0}_{m \times n}$	The $n \times 1$ vector and $m \times n$ matrix of all zeros; subscript is omitted when it is clear from context.
$A^\top, A^{-1}, A^\dagger$	The transpose, inverse, and pseudoinverse of the matrix $A$ respectively.
$A_{ij}, v_i$	The $i, j$ -th entry of the matrix $A$ and the $i$ -th element of a vector $v$ respectively.
$\lambda_i(A)$	The $i$ -th eigenvalue of the matrix $A$ .
$\sigma(A)$	The set of eigenvalues of the matrix $A$ .
$\text{blkdiag}(A, B)$	The block diagonal matrix with matrices $A$ and $B$ on its diagonal.
$\text{col}(v_1, v_2), \text{col}(A, B)$	The vertical concatenation of vectors $v_1, v_2$ or matrices $A, B$ .
$\mathbb{C}$	The field of complex numbers.
$\text{diag}(v)$	The diagonal matrix with $v$ on its main diagonal.
$\nabla f(x)$	The gradient $\nabla f : \mathbb{R}^n \rightarrow \mathbb{R}^n$ of the differentiable function $f : \mathbb{R}^n \rightarrow \mathbb{R}$ .
$\text{Im}(A)$	The column-space of the matrix $A \in \mathbb{R}^{m \times n}$ , i.e., $\text{Im}(A) := \{Ax   x \in \mathbb{R}^n\}$ . It could also be denoted as $\text{range}(A)$ .
$I_n$	The $n \times n$ identity matrix, subscript is omitted when it is clear from context.

$\text{null}(A)$	The null-space of the matrix $A \in \mathbb{R}^{m \times n}$ , i.e., $\text{null}(A) := \{x \in \mathbb{R}^n   Ax = \mathbb{0}_m\}$ . It could also be denoted as $\text{kerr}(A)$ .
$\text{nullity}(A)$	The nullity of the matrix $A$ .
$n_+(A), n_0(A), n_-(A)$	The number of positive, zero, and negative eigenvalues of $A \in \mathbb{R}^{n \times n}$ respectively; $n_0(A) = \text{nullity}(A)$ .
$\mathbb{R}$	The field of real numbers.
$\text{rank}(A)$	The rank of the matrix $A$ .
$\text{Re}(c), \text{Im}(c)$	The real and imaginary components of the complex number $c \in \mathbb{C}$ .
$\mathbb{S}^n$	The set of symmetric matrices in $\mathbb{R}^{n \times n}$ .
$\emptyset$	The empty set.
$\ \cdot\ _p$	The $\ell_p$ norm in $\mathbb{R}^n$ .
$ \cdot $	The absolute value of a real number.

# Chapter 1

## Introduction

### 1.1 Motivation

High voltage direct current (HVDC) transmission has been in use since the early 1950s with first HVDC cable link installed between mainland Sweden and Gotland Island [1]. Most of the HVDC transmission today possess a “point-to-point” configuration that connects two separate AC systems or two points of a single AC system [2]. Point-to-point HVDC transmission has been employed for long-distance transport of electrical energy, for interconnection of two AC systems that are operating at different frequencies or that are not synchronized, and for controllable power exchange between two AC systems [3]. On the other hand, a meshed interconnection of AC systems using HVDC lines is referred to as multi-terminal HVDC (MTDC) system.

Over the years, the thyristor-based line commutated converter (LCC) HVDC transmission matured to constitute the bulk of the planned and installed HVDC transmission capacity around the world with more than 150 point-to-point worldwide installations [4]. Although most of the installed LCC-HVDC systems possess point-to-point configuration, there are two operational exceptions; (1) the SACOI interconnection and (2) the Hydro-Quebec-New-England interconnection, whereby both systems have more than two points of connections to AC systems [5]. Even though both projects possess MTDC system topology, they are not considered truly meshed as the power flow in both projects is unidirectional from generation to load centers. For LCC-MTDC systems, power reversal necessitates reversing the DC voltage polarity. Since a terminal may be connected to more than one terminal in an MTDC topology, reversing voltage at one terminal produces undesirable changes in power flow in other lines. In addition to power reversal complexity, the LCC technology is bound by other limitations which hinder expanding its utilization in meshed MTDC systems such as slow response time, commutation failures, and infeasible connection to weak AC systems [4].

The advent of voltage source converters (VSC) has paved the way forward to developing controllable VSC-MTDC systems. This is mainly because of its self-commutating switches (IGBT) which (1) allow for a faster response, (2) enable independent control of active and reactive power, (3) facilitate paralleling on the DC side, and (4) permit instantaneous reverse of power flow through reversing the direction of current flow instead of reversing the DC voltage polarity [6], [7]. The VSC offers other gains such as ease of operation with weak AC systems, black start capability, and reduced footprint, etc [8].

MTDC systems offer a wide range of advantages over point-to-point links such as (1) improved reliability of the overall system, (2) reduced capacity and reserve capacity of generation units in the connected AC areas, (3) reduced curtailment of windfarms, (4) reduced variability in renewable generation due to integration of multiple renewable energy generating areas to the grid, (5) ease of maintenance as power can be rerouted through the meshed grid, and (6) facilitation of power exchange and trading between AC areas [9].

The deployment of VSC-MTDC systems is hindered by technical challenges such as (1) developing fast (within 1 ms) protection systems that detect DC side faults and identify respective faulty lines, (2) employing very fast (within 2 ms) fault current interruption mechanisms using fault-blocking converters or DC circuit breakers, and (3) controlling MTDC system variables (i.e., voltage, current, and power) to meet shared control goals (e.g., frequency control of connected AC systems) while meeting grid constraints (e.g., power flow in DC lines) [8], [9]. In this thesis, we tackle the third technical challenge: control of MTDC systems.

## 1.2 Literature Review

Different control strategies of MTDC systems have been proposed in the literature. Two general categories of control methods are mostly used: Voltage Margin Method (VMM) and Voltage Droop Method (VDM) [10]. The basic form of VMM and VDM is decentralized whereby each converter relies on local information without the need for communication between converters. A review of VMM and several VDM approaches is summarized in [11].

In VMM, each converter is given a marginal offset in its DC reference voltage such that one converter (slack converter) is responsible for maintaining DC voltage at a desired level to maintain power balance in the network while other converters operate at constant power mode [12]. In the case whereby the slack converter can no longer inject/absorb the real power needed to control the DC voltage, another converter will be assigned to operate as the slack converter. In VDM's basic form, all converters (or more than one converter) in the MTDC network participate in DC voltage control by adjusting their injected/absorbed real power into the MTDC network based on

a predefined droop [13]. A higher droop coefficient means that the converter will inject/absorb more real power given a DC voltage deviation.

With the increasing penetration of asynchronous generation, the effective inertia of AC systems is reduced and systems' frequency have become more volatile to disturbances. Hence, AC system stability necessitates the need for fast frequency support from other AC systems, which can be achieved by interconnecting them via an MTDC system [9]. If the frequency drops (rises) due to power imbalance at the AC side, the MTDC system responds by transferring power between AC systems; injecting more (less) or extracting less (more) real power into the disturbed AC system. The collective response of AC systems to power imbalance in any of them distributes the associated frequency deviation over the systems connected. This is referred to as primary frequency control of AC systems connected via an MTDC system [14].

In [15] and [16], a decentralized voltage control scheme is proposed whereby the voltage of the converter is proportionally adjusted with respect to frequency deviation of the AC system connected to it. In [17], a decentralized power control scheme is proposed whereby power injected from the AC system is proportional to DC voltage deviation and to frequency deviation of the respective AC system. The proposed controller is proven to stabilize the equilibrium of the closed-loop system such that primary frequency control action is fairly distributed among the generators, and the deviation of AC frequency and DC voltages are quantified and bounded. In [18], a distributed voltage control scheme is proposed which eliminates the differences in frequency variations as compared to that proposed in [15]. In [19], a distributed consensus-based controller is proposed which modifies the power injected by each area into the MTDC grid as a function of frequency deviations of neighboring AC areas. However, this controller requires a slack bus to maintain power balance in the MTDC system which limits distributing the primary frequency reserves over all AC systems.

The class of controllers presented above do not identify a quantifiable objective (cost) to be met (minimized) at steady state. Hence, although the proposed controller achieves its objective, it may be simultaneously compromising operation at an optimal steady state<sup>1</sup>. An optimal controller drives the system to a steady state which achieves defined control objectives while maintaining optimal operation.

Optimal controllers can be classified into two main categories: offline optimization and online optimization. In offline optimization, optimal setpoints are computed based on a steady-state system model and forecasts of disturbances which are then fed to classical tracking controllers [20], [21]. In contrast, online optimization incorporates real-time feedback into the computation of optimal set-points such that the system

---

<sup>1</sup>The optimal steady state of the system is specified by the solution of a defined constrained optimization problem.

converges to a cost-minimizing operating point [22]–[29]. The latter reduces sensitivity to steady-state model uncertainty and eliminates sub-optimal operation caused by discrepancies between forecasted and real-time disturbances. The linear-convex optimal steady state control (LC-OSS) [30] is an online feedback-based control framework which facilitates developing dynamic controller designs that regulate a linear time-invariant (LTI) system to a cost-minimizing and constraint-satisfying operating point in the presence of unmeasured disturbances.

### 1.3 Contributions

In this thesis, we adopt the LC-OSS framework to control MTDC systems. This thesis makes three primary contributions:

- We prove that the LC-OSS control encompasses some of the existing MTDC controllers in the literature. We recover two different MTDC controllers; a distributed power consensus controller and a decentralized voltage controller. We also provide a stability analysis of the MTDC system closed by each of the LC-OSS controllers.
- We propose an MTDC LC-OSS controller which regulates the VSC power set-points that control the AC-DC power transfer between AC systems to drive the MTDC system to an optimal operating point dictated by an optimization problem. We define a convex optimization problem that achieves the following control objectives: (1) minimize the frequency deviation in all AC systems in response to unmeasured power load variations happening in some of them, (2) minimize the total power loss in HVDC systems, and (3) enforce the HVDC link currents to be within acceptable upper and lower current limits. We then provide a stability analysis of the system with a simplified OSS controller that only achieves the first objective.
- We apply the proposed controller to an MTDC test system. We evaluate the controller’s performance based on a time-domain simulation in MATLAB/Simulink environment and verify that the controller is able to drive the system to the equilibrium corresponding to the solution of an optimization problem.

### 1.4 Thesis Layout

This thesis is organized as follows:

- In Chapter 2, we provide a summary of the mathematical and control theory background and tools needed for the remainder body of the thesis.
- In Chapter 3, we develop the state space model of a generic MTDC system.

- In Chapter 4, we apply the OSS control framework to MTDC systems. We first show that the LC-OSS control recovers some of the existing MTDC controllers in the literature. Then, we identify the control objectives and propose the MTDC-OSS controller accordingly. We finally provide a stability analysis of the system closed by a simplified version of the OSS controller.
- In Chapter 5, we provide time-domain simulation results of applying the proposed LC-OSS controller to a test system and evaluate the controller's performance.
- In Chapter 6, we provide a conclusion of this thesis and point out future research directions.

## Chapter 2

# Optimization and Control Background

In this chapter, we present background information on convex optimization, linear algebra, and linear control theory. We also reproduce the derivation of linear-convex optimal steady state control which is a core building block of this thesis.

### 2.1 Convex Optimization

Our MTDC control problem will be formulated as a convex optimization problem; this section recalls the basics of general optimization problems, and convex optimization in particular [31].

#### 2.1.1 Optimization Problems

An *optimization problem* is a problem of determining a vector (or set of vectors) of *decision variables*  $x \in \mathbb{R}^n$  that minimizes a cost function  $f : \mathbb{R}^n \rightarrow \mathbb{R}$  defined as

$$\underset{x \in \mathbb{R}^n}{\text{minimize}} \quad f(x), \tag{2.1}$$

which we refer to as the *objective function*.

We refer to a vector which minimizes the objective function as a *minimizer* or an *optimizer*  $x^* \in \mathbb{R}^n$  and to its corresponding cost  $f(x^*)$  as the *optimal value* satisfying  $f(x^*) \leq f(x)$  for all  $x \in \mathbb{R}^n$ . We denote by the set of minimizers as

$$\underset{x \in \mathbb{R}^n}{\text{argmin}} \quad f(x).$$

Problem (2.1) is an *unconstrained* optimization problem as there are no restrictions on the decision variable which may be any element in  $\mathbb{R}^n$ . In many cases, *constraints*

restrict the decision variable to belong to a set of permissible options. The set of permissible options is denoted as the *feasible set* or the *constraint set*  $\mathcal{C} \subseteq \mathbb{R}^n$ . Hence, a *constrained optimization* problem can be generally formulated as

$$\begin{aligned} & \underset{x \in \mathbb{R}^n}{\text{minimize}} && f(x) \\ & \text{subject to} && x \in \mathcal{C}. \end{aligned}$$

The set of minimizers of the constrained optimization problem becomes

$$\underset{x \in \mathbb{R}^n}{\text{argmin}} \quad \{f(x) \mid x \in \mathcal{C}\}.$$

The feasible region  $\mathcal{C}$  is often algebraically described by a set of functions  $g_i : \mathbb{R}^n \rightarrow \mathbb{R}$ ,  $i \in \{1, \dots, n_{ic}\}$ , that define *inequality constraints*, and a set of functions  $h_i : \mathbb{R}^n \rightarrow \mathbb{R}$ ,  $i \in \{1, \dots, n_{ec}\}$ , that define *equality constraints* such that

$$\mathcal{C} := \left\{ x \in \mathbb{R}^n \mid g_i(x) \leq 0 \text{ for all } i \in \{1, \dots, n_{ic}\}, h_i(x) = 0 \text{ for all } i \in \{1, \dots, n_{ec}\} \right\}.$$

Representing the feasibility set  $\mathcal{C}$  by its algebraic description, the constrained optimization problem becomes

$$\begin{aligned} & \underset{x \in \mathbb{R}^n}{\text{minimize}} && f(x) \\ & \text{subject to} && g_i(x) \leq 0, \quad \text{for all } i \in \{1, \dots, n_{ic}\}, \\ & && h_i(x) = 0, \quad \text{for all } i \in \{1, \dots, n_{ec}\}. \end{aligned} \tag{2.2}$$

### 2.1.2 Convexity (Sets, Functions, and Optimization)

A set  $\mathcal{C}$  is said to be a *convex set* if a line segment between any two points in  $\mathcal{C}$  lies in  $\mathcal{C}$ . Algebraically, if  $\mathcal{C}$  is convex, then for any  $x, y \in \mathcal{C}$  and any  $\lambda \in [0, 1]$ , we have

$$\lambda x + (1 - \lambda)y \in \mathcal{C}.$$

A function  $f : \mathbb{R}^n \rightarrow \mathbb{R}$  is said to be a *convex function* if the domain of  $f$  is a convex set, and the line segment between any two points on the graph of the function lies above the graph of  $f$ . Algebraically, if domain of  $f$  forms a convex set, then  $f$  is convex if for any  $x, y \in \text{dom} f$  and  $\lambda \in [0, 1]$

$$f(\lambda x + (1 - \lambda)y) \leq \lambda f(x) + (1 - \lambda)f(y). \tag{2.3}$$

A function is said to be *strictly convex* if (2.3) is a strict inequality for  $x \neq y \in \text{dom} f$  and  $\lambda \in (0, 1)$ .

The optimization problem (2.2) is said to be a *convex optimization problem* if the following requirements are satisfied:

1. the objective function  $f$  is convex,
2. the inequality constraint functions  $g_i$ , for  $i \in \{1, \dots, n_{ic}\}$ , are convex, and
3. the equality constraint functions  $h_i$ , for  $i \in \{1, \dots, n_{ec}\}$ , are affine.

The affine equality constraint functions  $h_i(x)$ , for  $i \in \{1, \dots, n_{ec}\}$  can be equivalently represented as  $Ax = b$  where  $A \in \mathbb{R}^{n_{ec} \times n}$  and  $b \in \mathbb{R}^{n_{ec}}$ . Therefore, a convex optimization problem can be represented as

$$\begin{aligned} & \underset{x \in \mathbb{R}^n}{\text{minimize}} && f(x) \\ & \text{subject to} && g_i(x) \leq 0, \quad \text{for all } i \in \{1, \dots, n_{ic}\} \\ & && Ax = b. \end{aligned} \tag{2.4}$$

### 2.1.3 The Karush-Kuhn-Tucker Conditions

For the convex optimization problem (2.4), there exists a set of conditions that are necessary and sufficient for optimality given that the optimization problem satisfies a so-called constraint qualification requirement. These conditions are referred to as: *The Karush-Kuhn-Tucker (KKT) Conditions*.

A qualification requirement for the KKT to be necessary and sufficient for optimality is called *Slater's constraint qualification*. The problem (2.4) is said to satisfy Slater's constraint qualification if there exists a *strictly feasible* point, i.e., a point  $\tilde{x}$  satisfying

$$g_i(\tilde{x}) < 0, \quad \text{for all } i \in \{1, \dots, n_{ic}\}, \quad \text{and } A\tilde{x} = b.$$

Assuming (2.4) satisfies Slater's constraint qualification,  $x^*$  is optimal if and only if there exists  $\lambda^* \in \mathbb{R}^{n_{ic}}$  and  $\nu^* \in \mathbb{R}^{n_{ec}}$  such that the KKT conditions

$$g_i(x^*) \leq 0, \quad \text{for all } i \in \{1, \dots, n_{ic}\} \quad \text{and } Ax^* = b, \tag{2.5a}$$

$$\lambda^* \geq 0, \tag{2.5b}$$

$$0 = \nabla f(x^*) + A^\top \nu^* + \sum_{i=1}^{n_{ic}} \lambda_i^* \nabla g_i(x^*), \tag{2.5c}$$

$$0 = \lambda_i^* g_i(x^*), \tag{2.5d}$$

are satisfied. Equation (2.5a) represents the primal feasibility conditions, (2.5b) represents the dual feasibility condition, (2.5c) represents the gradient condition, and (2.5d) represents the complementary slackness condition.

## 2.2 Linear-Convex Optimal Steady-State Control

This section reproduces the derivation of the LC-OSS control framework [30]. The framework produces output feedback controllers for an LTI system such that the system is asymptotically driven to an optimal steady-state. The optimal steady-state is defined to be the equilibrium corresponding to the output that minimizes a defined convex optimization problem. The LC-OSS control framework is an online optimization which processes real time measurements to guarantee an optimal operation despite constant unmeasured exogenous disturbance.

Consider a continuous-time LTI system subject to an unknown constant exogenous disturbance  $w \in \mathbb{R}^{n_w}$  which is given by

$$\begin{aligned} \dot{x} &= Ax + Bu + B_w w, & x(0) &\in \mathbb{R}^n \\ y &= Cx + Du + D_w w. \end{aligned} \tag{2.6}$$

with states  $x \in \mathbb{R}^n$ , input  $u \in \mathbb{R}^m$ , and output  $y \in \mathbb{R}^p$ .

We denote by  $\bar{y}$  the output generated by the equilibrium states  $\bar{x}$  and inputs  $\bar{u}$  for a fixed disturbance  $w$ , where  $\bar{x}$ ,  $\bar{u}$ , and  $\bar{y}$  satisfy

$$0 = A\bar{x} + B\bar{u} + B_w w, \tag{2.7a}$$

$$\bar{y} = C\bar{x} + D\bar{u} + D_w w. \tag{2.7b}$$

We define  $\bar{Y}(w)$  to be the set of all achievable equilibrium outputs  $\bar{y}$  for a fixed disturbance  $w$  as

$$\bar{Y}(w) := \{\bar{y} \in \mathbb{R}^p \mid \exists (\bar{x}, \bar{u}) \text{ such that } (\bar{x}, \bar{u}, \bar{y}) \text{ satisfy (2.7a) and (2.7b)}\}.$$

The objective of an LC-OSS controller is to drive the system to an equilibrium corresponding to the optimizer of the problem

$$\underset{y \in \mathbb{R}^p}{\text{minimize}} \quad f(y, w) \tag{2.8a}$$

$$\text{subject to} \quad y \in \bar{Y}(w) \tag{2.8b}$$

$$Hy = Lw. \tag{2.8c}$$

The feasible set is defined by (2.8b) which represents the equilibrium constraint, and by (2.8c) which represents  $n_{\text{eq}}$  engineering equality constraints determined by the matrices  $H \in \mathbb{R}^{n_{\text{eq}} \times p}$  and  $L \in \mathbb{R}^{n_{\text{eq}} \times n_w}$ . The  $n_{\text{eq}}$  constraints represent additional constraints that are imposed by the designer.

**Assumption 2.2.1.** The LC-OSS control framework requires:

1. the function  $f$  to be differentiable and strictly convex in  $y$  for every  $w$ ,

2. the feasible region to have a non-empty relative interior, and
3. the optimizer  $y^*$  to exist, therefore  $y^*$  is unique as  $f$  is strictly convex.

Next, we reformulate (2.8b) such that it can be represented in standard equality form. First, we define the set  $\mathcal{Z}(w) \subseteq \mathbb{R}^{n+m}$  which contains all possible solutions  $(\bar{x}, \bar{u})$  to (2.7a) for a given  $w$ . Since  $\mathcal{Z}$  is an affine subspace, it can be written as a sum of a unique subspace and a non-unique offset vector such that

$$\mathcal{Z}(w) := \{z \in \mathbb{R}^{n+m} \mid \exists \alpha \in \mathbb{R}^\bullet \text{ such that } z = \tilde{z} + \mathcal{N}\alpha\},$$

where  $\tilde{z}$  is a particular solution and  $\mathcal{N} \in \mathbb{R}^{(n+m) \times \bullet}$  is defined such that  $\text{range } \mathcal{N} = \text{null} \begin{bmatrix} A & B \end{bmatrix}$ .<sup>1</sup>

Hence, the affine set  $\bar{Y}(w)$  can also be written as a sum of a unique subspace and a non-unique offset vector  $\tilde{y}(w)$  such that

$$\begin{aligned} \bar{Y}(w) &= \{y \in \mathbb{R}^p \mid y = C\bar{x} + D\bar{u} + D_w w \text{ and } \text{col}(\bar{x}, \bar{u}) \in \mathcal{Z}(w)\} & (2.9) \\ &= \{y \in \mathbb{R}^p \mid \exists \alpha \in \mathbb{R}^\bullet \text{ such that } y = \begin{bmatrix} C & D \end{bmatrix} \mathcal{N}\alpha + \begin{bmatrix} C & D \end{bmatrix} \tilde{z} + D_w w\} \\ &= \{y \in \mathbb{R}^p \mid \exists \alpha \in \mathbb{R}^\bullet \text{ such that } y = G\alpha + \tilde{y}(w)\}, \end{aligned}$$

where  $G \in \mathbb{R}^{p \times \bullet}$  is defined such that  $G := \begin{bmatrix} C & D \end{bmatrix} \mathcal{N}$  and  $\tilde{y}(w) := \begin{bmatrix} C & D \end{bmatrix} \tilde{z} + D_w w$ .

Next, we define matrix  $G_\perp \in \mathbb{R}^{l \times p}$  with  $l := p - \text{rank}(G)$  such that

$$\text{null}(G_\perp) = \text{range}(G). \quad (2.10)$$

Left multiplying the expression of  $y$  in (2.9) by  $G_\perp$ , we get

$$\bar{Y}(w) = \{y \in \mathbb{R}^p \mid G_\perp y = b(w)\}, \quad (2.11)$$

where  $b(w) := G_\perp \tilde{y}(w)$ . Substituting the equality constraint (2.8b) by (2.11), the optimization problem (2.8) becomes

$$\begin{aligned} &\underset{y \in \mathbb{R}^p}{\text{minimize}} && f(y, w) \\ &\text{subject to} && G_\perp y = b(w) \\ &&& Hy = Lw. \end{aligned} \quad (2.12)$$

Since we assumed the existence of a strictly feasible point (as per Assumption 2.2.1-2), Slater's condition holds which guarantees that the KKT conditions are necessary and sufficient for optimality. Therefore, for every  $w$ , there exists a unique optimal primal optimizer  $y^*$  and optimal dual optimizers  $(\sigma^*, \mu^*)$  such that  $(y^*, \sigma^*, \mu^*)$  satisfy

<sup>1</sup>The symbol  $\bullet$  in  $\mathbb{R}^\bullet$  indicates that the dimension of the vector space is unspecified.

the KKT conditions

$$\text{Gradient Condition: } \nabla f(y^*, w) + G_{\perp}^{\top} \sigma^* + H^{\top} \mu^* = \mathbb{0}, \quad (2.13a)$$

$$\text{Equilibrium Feasibility Condition: } G_{\perp} y^* - b(w) = \mathbb{0}, \quad (2.13b)$$

$$\text{Engineering Feasibility Condition: } Hy^* - Lw = \mathbb{0}. \quad (2.13c)$$

Rearranging the KKT gradient condition (2.13a), we get

$$G_{\perp}^{\top}(-\sigma^*) = \nabla f(y^*, w) + H^{\top} \mu^*.$$

Taking the orthogonal complement of both sides of (2.10) such that  $\text{range}(G_{\perp}^{\top}) = \text{null}(G^{\top})$ , we deduce that

$$\left( \nabla f(y^*, w) + H^{\top} \mu^* \right) \in \text{range}(G_{\perp}^{\top}) = \text{null}(G^{\top}).$$

Hence, the existence of  $(y^*, \sigma^*, \mu^*)$  which satisfies the gradient condition (2.13a) is equivalent to the existence of a pair  $(y^*, \mu^*)$  which satisfies

$$G^{\top} \left( \nabla f(y^*, w) + H^{\top} \mu^* \right) = \mathbb{0}. \quad (2.14)$$

With the assumption that we have an error measurement of engineering violations  $Hy - Lw$ , [30] introduces an *optimality model* which is a dynamic filter of the form

$$\begin{aligned} \dot{\mu} &= Hy - Lw, \\ \epsilon &= G^{\top} \left( \nabla f(y, w) + H^{\top} \mu \right). \end{aligned} \quad (2.15)$$

The idea of the filter is that  $\mu$  and the error variable  $\epsilon$  should together provide a measure of the *optimality gap*. Hence, at steady state, we need  $\dot{\mu} = 0$  and  $\epsilon = 0$  to ensure satisfying (2.13c) and (2.13a) respectively. Employing an integrator to  $\epsilon$  such that

$$\dot{\eta} = \epsilon \quad (2.16)$$

and proposing a stabilizer<sup>2</sup> to the cascaded system represented by the LTI system (2.6), the optimality model (2.15), and the integral controller (2.16) will ensure satisfying the KKT conditions (2.13b), (2.13c), and (2.14). The cascaded system in Figure 2.1 represent the block diagram of the general LC-OSS control architecture.

<sup>2</sup>A feedback stabilizer  $u = f(x, \mu, \eta)$  drives  $\dot{x}$ ,  $\dot{\mu}$ , and  $\dot{\eta}$  to zero at steady state.

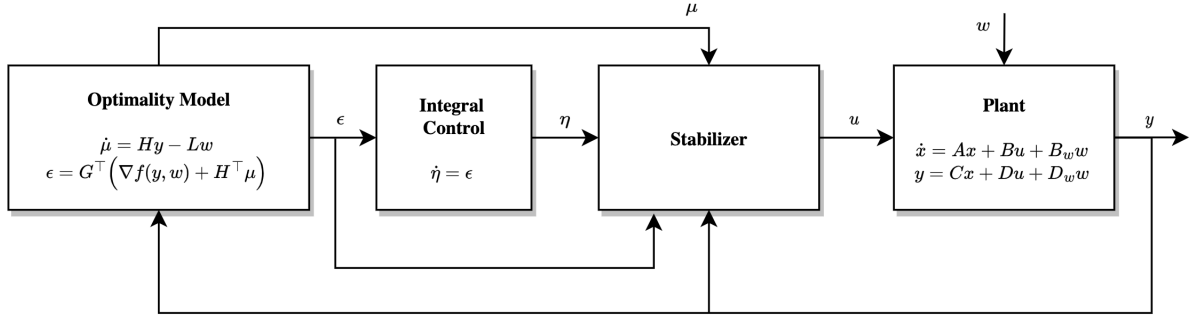


Figure 2.1: Block diagram of general OSS control architecture

## 2.3 Mathematical and Control Theory Tools

This section recalls some of the mathematical and linear control theory tools used in the main body of this thesis. Proofs of theorems are not reproduced, we refer the reader to the references indicated for the full proof of the theorem.

**Definition 2.3.1** (Hurwitz matrix). Matrix  $A \in \mathbb{R}^{n \times n}$  is called a *Hurwitz matrix* if every eigenvalue of  $A$  has strictly negative real part, i.e.,  $\text{Re}(\lambda_i(A)) < 0$  for  $i = 1, \dots, n$ .

**Definition 2.3.2.** (Definite Matrices) A square matrix  $A \in \mathbb{R}^{n \times n}$  is

1. *Positive definite* ( $A \succ 0$ ) if  $A = A^\top$  and  $v^\top A v > 0$  for all  $v \in \mathbb{R}^n \setminus \{0\}$ .
2. *Positive semi-definite* ( $A \succeq 0$ ) if  $A = A^\top$  and  $v^\top A v \geq 0$  for all  $v \in \mathbb{R}^n$ .

**Theorem 2.3.1** (Theorem 4.1.10, [32]). *Given a square matrix  $A \in \mathbb{R}^{n \times n}$ , the eigenvalues of  $A$  are:*

1. *non-negative real if and only if  $A \succeq 0$ , and*
2. *positive real if and only if  $A \succ 0$ .*

**Definition 2.3.3** (Similar matrices). Two square matrices  $A$  and  $B$  are *similar* if there exists an invertible matrix  $S$  such that  $A = S^{-1}BS$ .

**Theorem 2.3.2** (Theorem 1.3.3, [32]). *Let  $A$  and  $B$  be similar matrices, then  $A$  and  $B$  have the same characteristic polynomial, i.e.,  $\sigma(A) = \sigma(B)$ <sup>3</sup>.*

**Corollary 2.3.1.** *Given two matrices  $A \succ 0$  and  $B \succeq 0$ , then,  $\sigma(AB) = \sigma(A^{1/2}BA^{1/2}) \subseteq [0, +\infty)$ .*

*Proof.*  $AB$  and  $A^{1/2}BA^{1/2}$  are similar with  $S = A^{1/2}$  as per Definition 2.3.3, then  $\sigma(AB) = \sigma(A^{1/2}BA^{1/2}) \subseteq [0, +\infty)$ .  $\square$

<sup>3</sup>The set of eigenvalues of the matrix  $A$  is denoted by  $\sigma(A)$  as defined in the List of Symbols.

**Definition 2.3.4** (Congruent matrices). Two square matrices  $A$  and  $B$  are *congruent* if there exists an invertible matrix  $S$  such that  $A = S^\top BS$ .

**Definition 2.3.5** (Signature of a matrix). The *signature* of a matrix  $A \in \mathbb{S}^n$  is the number of positive, negative, and zero eigenvalues of  $A$ , that is the triple:  $(n_+(A), n_-(A), n_0(A))$ .

**Theorem 2.3.3** (Theorem 9.13, [33]). *Let  $A$  and  $B$  be congruent real symmetric matrices, then  $A$  and  $B$  have the same signature, that is*

$$\begin{aligned} n_+(A) &= n_+(B), \\ n_0(A) &= n_0(B), \text{ and} \\ n_-(A) &= n_-(B). \end{aligned}$$

**Corollary 2.3.2.** *Given two matrices  $A \succ 0$  and  $B \succeq 0$ , then, the number of zero eigenvalues of  $AB$  is equal to that of  $B$  i.e.,  $n_0(AB) = n_0(B)$ .*

*Proof.* It is evident that  $A^{1/2}BA^{1/2}$  and  $B$  are congruent with  $S = A^{-1/2}$  as per Definition 2.3.4. Hence, by Theorem 2.3.3,  $n_0(A^{1/2}BA^{1/2}) = n_0(B)$ . And since  $\sigma(AB) = \sigma(A^{1/2}BA^{1/2})$  (by Corollary 2.3.1), then  $n_0(AB) = n_0(B)$ .  $\square$

**Corollary 2.3.3.** *Given two matrices  $A \succeq 0$  and  $B \succ 0$ , then,*

1. *the eigenvalues of  $AB$  are non-negative, i.e.,  $\sigma(AB) \subseteq [0, +\infty)$ , and*
2. *the number of zero eigenvalues of  $AB$  is equal to that of  $A$ , i.e.,  $n_0(AB) = n_0(A)$ .*

*Proof.* The proof of Corollary 2.3.3 is similar to that of Corollary 2.3.2.  $\square$

**Definition 2.3.6** (Defective eigenvalue). A *defective eigenvalue* of a matrix  $A$  is one whose algebraic multiplicity is greater than its geometric multiplicity. Conversely, a *non-defective eigenvalue* is one whose algebraic multiplicity is equal to its geometric multiplicity.

**Theorem 2.3.4** (Theorem 4.6, [34]). *Given the autonomous continuous-time LTI system*

$$\dot{x} = Ax, \tag{2.17}$$

*and the Lyapunov equation defined such that*

$$A^\top P + PA + Q = 0,$$

*where  $A, P, Q \in \mathbb{R}^{n \times n}$  and  $P, Q$  are symmetric. Then,*

1. the system (2.17) is globally asymptotically stable, i.e.  $\operatorname{Re}(\lambda_i(A)) < 0$  for  $i = 1, \dots, n$ , if and only if  $P \succ 0$  and  $Q \succ 0$ , and
2. all the trajectories of the system (2.17) are bounded, i.e.  $\operatorname{Re}(\lambda_i(A)) \leq 0$  for  $i = 1, \dots, n$  and those with  $\operatorname{Re}(\lambda_i(A)) = 0$  are non-defective, if and only if  $P \succ 0$  and  $Q \succeq 0$ .

**Theorem 2.3.5** (Theorem 1.12, [35]). *Let  $X$  be a Hermitian matrix partitioned as:*

$$X = \begin{bmatrix} A & B \\ B^\top & C \end{bmatrix}$$

*in which  $A$  is square and nonsingular. Then,*

1.  $X \succ 0$  if and only if  $A \succ 0$  and  $C - B^\top A^{-1} B \succ 0$ , and
2.  $X \succeq 0$  if and only if  $A \succ 0$  and  $C - B^\top A^{-1} B \succeq 0$ .

## Chapter 3

# MTDC System Modeling

In this chapter, we develop the state space model of the MTDC system. In Section 3.1, we describe the overall network topology of the MTDC system by defining the graphs representing each of the DC and AC systems and their respective interconnection matrices (incidence matrices of HVDC systems and AC/DC interconnection vectors). In Section 3.2, we develop a state-space model of a generic HVDC network and highlight modelling assumptions. In Section 3.3 we develop the state-space model of the AC systems. And finally, we combine AC and DC models in a single aggregate state-space model in Section 3.4.

### 3.1 Network Topology

The topology of the MTDC network is described by a connected, undirected graph  $\mathcal{G} = (\mathcal{V}, \mathcal{E})$  where  $\mathcal{V}$  is the set of all system buses (DC and AC) and  $\mathcal{E}$  is the set of all system lines (DC and AC). The network is partitioned into a set of HVDC networks  $\mathcal{G}_{dc}$  and a set of AC networks  $\mathcal{G}_{ac}$ . The network topology of the MTDC system is represented in Figure 3.1.

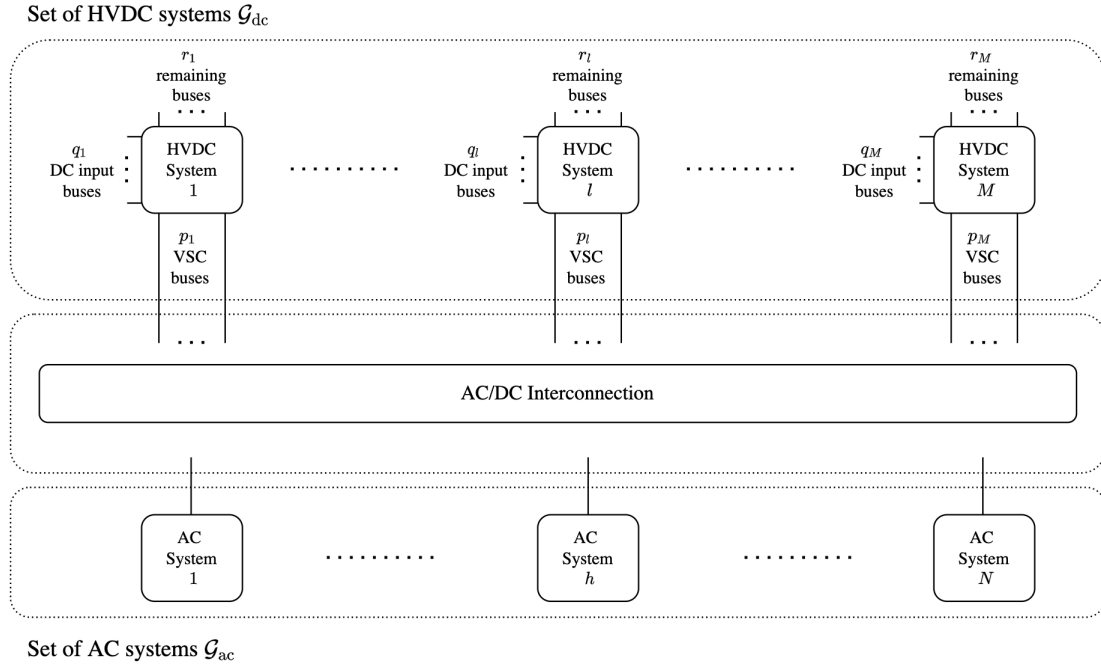


Figure 3.1: Network topology of the MTDC system

We assume that  $\mathcal{G}_{dc}$  consists of  $M$  disjoint, connected, undirected sub-graphs  $\mathcal{G}_{dc,l} = (\mathcal{V}_{dc,l}, \mathcal{E}_{dc,l})$  for  $l = 1, \dots, M$  whereby, for an HVDC network  $l$ ,  $\mathcal{V}_{dc,l}$  is the set of  $n_{dc,l}$  DC buses, and  $\mathcal{E}_{dc,l}$  is the set of  $m_{dc,l}$  lines each having its reference direction. The DC nodes are partitioned to three mutually exclusive subsets  $\mathcal{V}_{dc,l} := \mathcal{V}_{vsc,l} \cup \mathcal{V}_{in,l} \cup \mathcal{V}_{ld,l}$  where  $\mathcal{V}_{vsc,l}$  represents the set of  $p_l$  buses connected to voltage source converters,  $\mathcal{V}_{in,l}$  represents the set of  $q_l$  buses connected to DC input sources, and  $\mathcal{V}_{ld,l}$  represents the set of remaining  $r_l$  DC load buses. Each bus in  $\mathcal{V}_{vsc,l}$  is associated to one VSC. A DC interconnection (incidence) matrix  $F_{dc,l} \in \mathbb{R}^{n_{dc,l} \times m_{dc,l}}$  is associated with  $\mathcal{G}_{dc,l}$  and is defined such that

$$F_{dc,l} := [f_{ij}]_{(n_{dc,l} \times m_{dc,l})},$$

where for  $i = 1, \dots, n_{dc,l}$  and  $j = 1, \dots, m_{dc,l}$ ,  $f_{ij}$  is defined by

$$f_{ij} := \begin{cases} 1, & \text{if DC link } j \text{ is directed away from DC bus } i, \\ -1, & \text{if DC link } j \text{ is directed towards DC bus } i, \\ 0, & \text{otherwise.} \end{cases}$$

We assume that  $\mathcal{G}_{ac}$  consists of  $N$  disjoint vertices each representing an aggregate model of an AC system.

**Remark 3.1.1.** Extending the graph representation of AC systems to a full AC sys-

tem model is conceptually straightforward. However, this comes at the expense of increased notational complexity

For AC system  $h$  and HVDC system  $l$ , we define an interconnection vector  $c_{h,l} \in \mathbb{R}^{p_l}$  with components  $c_{h,l}^i$  defined by

$$c_{h,l}^i = 1, \quad \text{if VSC } i \text{ of HVDC system } l \text{ is connected to AC system } h.$$

Therefore, the interconnection vector  $c_h$  associated to every AC system is defined as

$$c_h = \text{col}(c_{h,1}, \dots, c_{h,M}). \quad (3.1)$$

## 3.2 HVDC System Model

### 3.2.1 Modeling of a Single HVDC System $l$

Consider an HVDC network  $l$  shown in Figure 3.2. Mapping the circuit diagram in Figure 3.2 to the overall system topology in Figure 3.1, the set of  $p_l$  VSC buses are on the top-left of the diagram, the set of  $q_l$  DC input sources are on the bottom of the diagram, and the set of  $r_l$  load buses are on the top right of the diagram. We assume that each of the DC buses is connected to a terminal shunt capacitor  $C_{\text{dc},l}^i$  for  $i = 1, \dots, n_{\text{dc},l}$ . We also assume that the HVDC network lines are modeled by a single  $\Pi$ -link with series resistance  $R_l^j$  and inductance  $L_l^j$ , and parallel capacitance  $C_{\Pi,l}^j$  and conductance  $G_{\Pi,l}^j$  for  $j = 1, \dots, m_{\text{dc},l}$ .

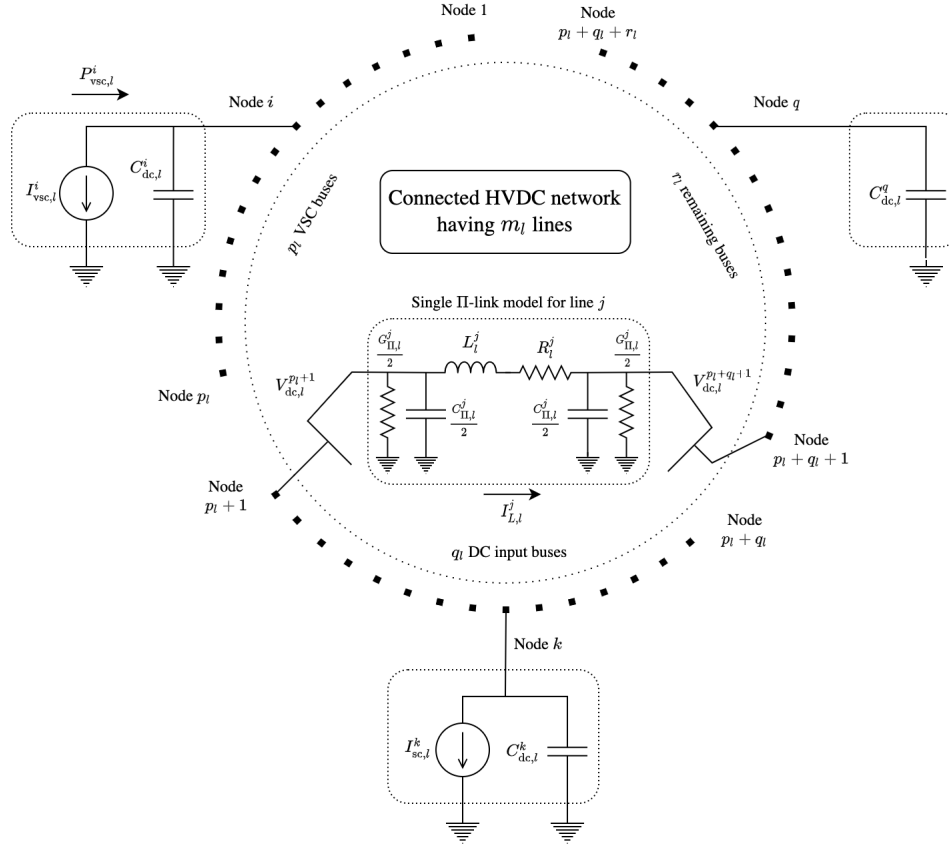
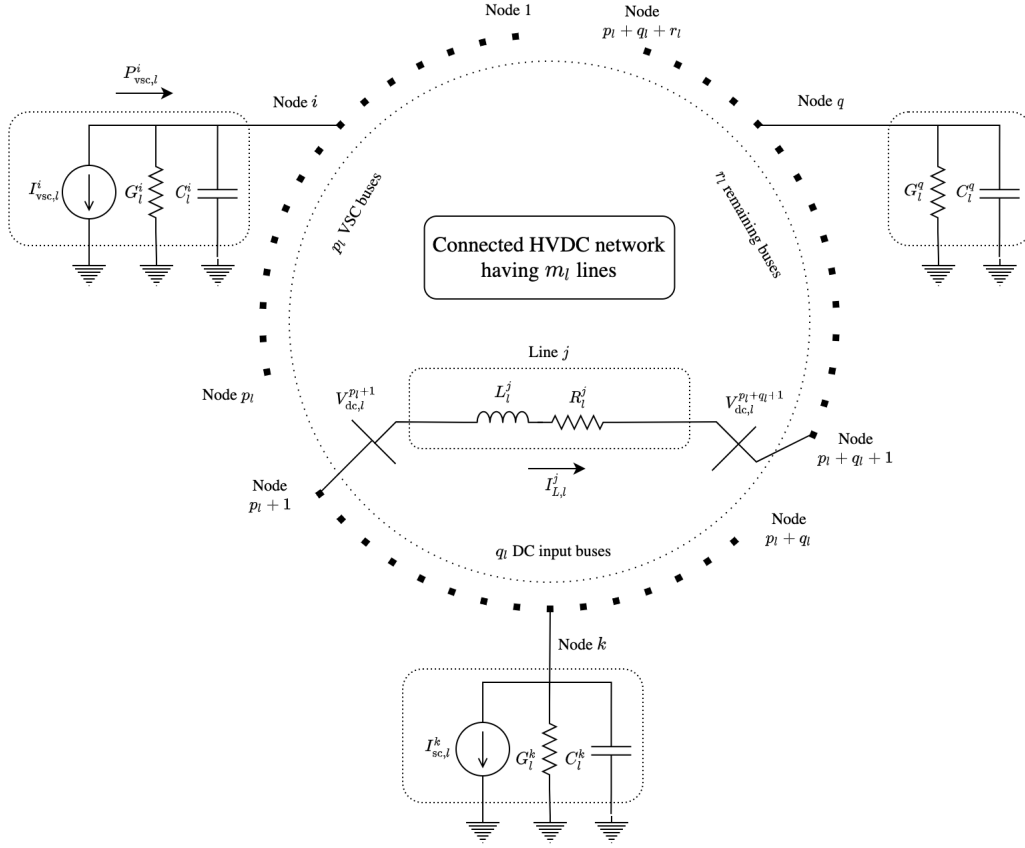

 Figure 3.2: Circuit diagram of HVDC system  $l$ 

Figure 3.2 can be further simplified to obtain an equivalent circuit network as in Figure 3.3 such that

$$\begin{aligned}
 [C_l^1, \dots, C_l^{n_{dc,l}}] &:= [C_{dc,l}^1, \dots, C_{dc,l}^{n_{dc,l}}] + \frac{1}{2} \left( \hat{F}_{dc,l} [C_{\Pi,l}^1, \dots, C_{\Pi,l}^{m_{dc,l}}]^\top \right)^\top \\
 [G_l^1, \dots, G_l^{n_{dc,l}}] &:= \frac{1}{2} \left( \hat{F}_{dc,l} [G_{\Pi,l}^1, \dots, G_{\Pi,l}^{m_{dc,l}}]^\top \right)^\top,
 \end{aligned}$$

where  $\hat{F}_{dc,l}$  is the absolute value of the incidence matrix  $F_{dc,l}$  such that

$$\hat{F}_{dc,l} := [ |f_{ij}| ]_{(n_{dc,l} \times m_{dc,l})}.$$


 Figure 3.3: Equivalent circuit diagram of HVDC system  $l$ 

Next, we define our system matrices  $C_l$  as such that

$$C_l := \text{diag}(C_l^1, \dots, C_l^{n_{\text{dc},l}}) := \text{blkdiag}(C_{\text{vsc},l}, C_{\text{in},l}, C_{\text{ld},l}) \quad (\text{in F}),$$

where

$$\begin{aligned} C_{\text{vsc},l} &:= \text{diag}(C_l^1, \dots, C_l^{p_l}), \\ C_{\text{in},l} &:= \text{diag}(C_l^{p_l+1}, \dots, C_l^{p_l+q_l}), \\ C_{\text{ld},l} &:= \text{diag}(C_l^{p_l+q_l+1}, \dots, C_l^{m_{\text{dc},l}}). \end{aligned}$$

The matrices  $G_l$ ,  $R_l$ , and  $L_l$  are defined such that

$$\begin{aligned} G_l &:= \text{diag}(G_l^1, \dots, G_l^{m_{\text{dc},l}}) \quad (\text{in } 1/\Omega), \\ R_l &:= \text{diag}(R_l^1, \dots, R_l^{m_{\text{dc},l}}) \quad (\text{in } \Omega), \\ L_l &:= \text{diag}(L_{l,1}, \dots, L_l^{m_{\text{dc},l}}) \quad (\text{in H}). \end{aligned}$$

From basic circuit theory [36], applying Kirchhoff's current law (KCL) and Kirchhoff's voltage law (KVL), we obtain the differential equations

$$\text{KCL: } C_l \frac{d}{dt} V_{\text{dc},l} + G_l V_{\text{dc},l} + \begin{bmatrix} I_{\text{vsc},l} \\ I_{\text{sc},l} \\ I_{\text{ld},l} \end{bmatrix} = -F_{\text{dc},l} I_{L,l}, \quad (3.2)$$

$$\text{KVL: } L_l \frac{d}{dt} I_{L,l} + R_l I_{L,l} = F_{\text{dc},l}^\top V_{\text{dc},l},$$

that describe the dynamics of the HVDC system in terms of DC bus voltages  $V_{\text{dc},l}(t)$  and DC line currents  $I_{L,l}(t)$ <sup>1</sup>.

The system state variables are defined as

$$V_{\text{dc},l} := \begin{bmatrix} V_{\text{dc},l}^1 \\ \vdots \\ V_{\text{dc},l}^{n_{\text{dc},l}} \end{bmatrix} \quad (\text{in V}), \quad I_{L,l} := \begin{bmatrix} I_{L,l}^1 \\ \vdots \\ I_{L,l}^{m_{\text{dc},l}} \end{bmatrix} \quad (\text{in A}),$$

and system input variables are defined as

$$I_{\text{vsc},l} := \begin{bmatrix} I_{\text{vsc},l}^1 \\ \vdots \\ I_{\text{vsc},l}^{p_l} \end{bmatrix}, \quad I_{\text{sc},l} := \begin{bmatrix} I_{\text{sc},l}^1 \\ \vdots \\ I_{\text{sc},l}^{q_l} \end{bmatrix}, \quad I_{\text{ld},l} := \begin{bmatrix} I_{\text{ld},l}^1 \\ \vdots \\ I_{\text{ld},l}^{r_l} \end{bmatrix} \quad (\text{in A}).$$

Representing (3.2) in a matrix format and rearranging, we get the state-space representation

$$\frac{d}{dt} \begin{bmatrix} V_{\text{dc},l} \\ I_{L,l} \end{bmatrix} = \begin{bmatrix} C_l^{-1} & \mathbb{0} \\ \mathbb{0} & L_l^{-1} \end{bmatrix} \begin{bmatrix} -G_l & -F_{\text{dc},l} \\ F_{\text{dc},l}^\top & -R_l \end{bmatrix} \begin{bmatrix} V_{\text{dc},l} \\ I_{L,l} \end{bmatrix} - \begin{bmatrix} C_l^{-1} \\ \mathbb{0} \end{bmatrix} \begin{bmatrix} I_{\text{vsc},l} \\ I_{\text{sc},l} \\ I_{\text{ld},l} \end{bmatrix}. \quad (3.3)$$

Finally, if all DC links are overhead lines, we can neglect the line conductance, hence (3.3) simplifies to

$$\frac{d}{dt} \begin{bmatrix} V_{\text{dc},l} \\ I_{L,l} \end{bmatrix} = \begin{bmatrix} \mathbb{0} & -C_l^{-1} F_{\text{dc},l} \\ L_l^{-1} F_{\text{dc},l}^\top & -L_l^{-1} R_l \end{bmatrix} \begin{bmatrix} V_{\text{dc},l} \\ I_{L,l} \end{bmatrix} - \begin{bmatrix} C_l^{-1} \\ \mathbb{0} \end{bmatrix} \begin{bmatrix} I_{\text{vsc},l} \\ I_{\text{sc},l} \\ I_{\text{ld},l} \end{bmatrix}. \quad (3.4)$$

The control input of the state-space model (3.4) is  $I_{\text{vsc},l}$  whereas the variable which can be independently controlled by the VSCs is the the power transferred between

<sup>1</sup>For conciseness, we will drop the time variable ( $t$ ) from HVDC systems' variables in the remaining body of the thesis.

the AC and DC systems  $P_{\text{vsc},l}$ . Therefore, require the below assumption to establish a relation between  $P_{\text{vsc},l}$  and  $I_{\text{vsc},l}$ .

**Assumption 3.2.1.** The power loss by the VSCs is neglected and the converter response is assumed to be instantaneous, i.e., injected power  $P_{\text{vsc},l}^i$  from the AC side is immediately and losslessly converted to DC power such that

$$P_{\text{vsc},l}^i = -V_{\text{dc},l}^i I_{\text{vsc},l}^i, \quad \text{for } i = 1, \dots, p_l. \quad (3.5)$$

Since the converter's power loss is negligible compared to that transferred by the VSCs, it is reasonable to ignore converter losses and to assume that VSCs are lossless. In addition, the VSC dynamics are orders of magnitudes faster than the primary frequency control dynamics of the AC systems, hence ignoring the converter dynamics and assuming that VSCs instantaneously track power commands dispatched by a controller is a justified assumption.

It should be noted that substituting (3.5) in (3.4), results in a non-linear state-space model. The following assumption linearizes the system model.

**Assumption 3.2.2.** The DC voltages  $V_{\text{dc},l}^i$  of VSC buses are approximated by  $V_{\text{dc},l}^i = V_{\text{dc},l}^{\text{nom}}$ , for  $i = 1, \dots, p_l$  such that

$$P_{\text{vsc},l}^i = -V_{\text{dc},l}^{\text{nom}} I_{\text{vsc},l}^i, \quad \text{for } i = 1, \dots, p_l.$$

For VSC buses, the voltages  $V_{\text{dc},l}^i$  do not significantly deviate from the nominal voltage  $V_{\text{dc},l}^{\text{nom}}$  as the acceptable deviation from the nominal voltage is less than 5% for most HVDC converters. Therefore, Assumption 3.2.2 will result in an error margin of approximately 5% in the control input commands  $P_{\text{vsc},l}^i$  dispatched to the VSCs. It should be noted that this assumption only holds for the power injection equation (3.5) and restricts the approximation to the control input  $P_{\text{vsc},l}^i$  only, we will continue to model  $V_{\text{dc},l}^i$  as a variable state for all HVDC buses.

Substituting this approximation into (3.4), we get the linearized state-space model

$$\frac{d}{dt} \begin{bmatrix} V_{\text{dc},l} \\ I_{L,l} \end{bmatrix} = \begin{bmatrix} \mathbb{0} & -C_l^{-1} F_{\text{dc},l} \\ L_l^{-1} F_{\text{dc},l}^\top & -L_l^{-1} R_l \end{bmatrix} \begin{bmatrix} V_{\text{dc},l} \\ I_{L,l} \end{bmatrix} - \begin{bmatrix} C_l^{-1} \\ \mathbb{0} \end{bmatrix} \begin{bmatrix} \frac{-1}{V_{\text{dc},l}^{\text{nom}}} P_{\text{vsc},l} \\ I_{\text{sc},l} \\ I_{\text{ld},l} \end{bmatrix},$$

where

$$P_{\text{vsc},l} := \text{col}(P_{\text{vsc},l}^1, \dots, P_{\text{vsc},l}^{p_l}) \quad (\text{in } W).$$

The above state and input variables can be divided to their steady state (marked

with a bar) and deviation components:

$$\begin{aligned} V_{\text{dc},l} &:= \bar{V}_{\text{dc},l} + v_{\text{dc},l}, \\ I_{L,l} &:= \bar{I}_{L,l} + i_{L,l}, \\ P_{\text{vsc},l} &:= \bar{P}_{\text{vsc},l} + \Delta P_{\text{vsc},l}, \\ I_{\text{sc},l} &:= \bar{I}_{\text{sc},l} + \Delta I_{\text{sc},l}, \\ I_{\text{ld},l} &:= \bar{I}_{\text{ld},l} + \Delta I_{\text{ld},l}. \end{aligned}$$

Extracting the deviation variables from the above state space representation, we get

$$\frac{d}{dt} \begin{bmatrix} v_{\text{dc},l} \\ i_{L,l} \end{bmatrix} = \begin{bmatrix} \mathbb{0} & -C_l^{-1} F_{\text{dc},l} \\ L_l^{-1} F_{\text{dc},l}^\top & -L_l^{-1} R_l \end{bmatrix} \begin{bmatrix} v_{\text{dc},l} \\ i_{L,l} \end{bmatrix} - \begin{bmatrix} C_l^{-1} \\ \mathbb{0} \end{bmatrix} \begin{bmatrix} \frac{-1}{V_{\text{dc},l}^{\text{nom}}} \Delta P_{\text{vsc},l} \\ \Delta I_{\text{sc},l} \\ \Delta I_{\text{ld},l} \end{bmatrix},$$

where, for the HVDC system  $l$ ,  $v_{\text{dc},l}$  and  $i_{L,l}$  respectively represent the voltage deviation of the DC buses and the current deviation of the DC links,  $\Delta P_{\text{vsc},l}$  represents the power injection deviation by the VSCs, and  $\Delta I_{\text{sc},l}, \Delta I_{\text{ld},l}$  represent the current deviation in the remaining DC buses.

The above state space representation can be written as

$$\dot{x}_{\text{dc},l} = A_{\text{dc},l} x_{\text{dc},l} + B_{\text{dc},l} u_l + B_{\text{dc},l}^w w_{\text{dc},l},$$

with state, input, and disturbance vectors defined as

$$x_{\text{dc},l} := \begin{bmatrix} v_{\text{dc},l} \\ i_{L,l} \end{bmatrix} \in \mathbb{R}^{n_{\text{dc},l} + m_{\text{dc},l}}, \quad u_l := \Delta P_{\text{vsc},l} \in \mathbb{R}^{p_l}, \quad w_{\text{dc},l} := \begin{bmatrix} \Delta I_{\text{sc},l} \\ \Delta I_{\text{ld},l} \end{bmatrix} \in \mathbb{R}^{q_l + r_l},$$

and system matrices defined as

$$\begin{aligned} A_{\text{dc},l} &:= \begin{bmatrix} \mathbb{0} & -C_l^{-1} F_{\text{dc},l} \\ L_l^{-1} F_{\text{dc},l}^\top & -L_l^{-1} R_l \end{bmatrix}, \\ B_{\text{dc},l} &:= \begin{bmatrix} \frac{1}{V_{\text{dc},l}^{\text{nom}}} C_{\text{vsc},l}^{-1} \\ \mathbb{0} \end{bmatrix}, \\ B_{\text{dc},l}^w &:= \begin{bmatrix} \mathbb{0} \\ -\text{blkdiag}(C_{\text{in},l}, C_{\text{ld},l})^{-1} \\ \mathbb{0} \end{bmatrix}. \end{aligned}$$

### 3.2.2 Modeling of the Set of $M$ HVDC Systems

The state space representation of the  $M$  HVDC networks is

$$\dot{x}_{\text{dc}} = A_{\text{dc}}x_{\text{dc}} + B_{\text{dc}}u + B_{\text{dc}}^w w_{\text{dc}},$$

with state, input, and disturbance vectors defined as:

$$\begin{aligned} x_{\text{dc}} &:= \text{col}(x_{\text{dc},1}, \dots, x_{\text{dc},M}), \\ u &:= \text{col}(u_1, \dots, u_M), \\ w_{\text{dc}} &:= \text{col}(w_{\text{dc},1}, \dots, w_{\text{dc},M}), \end{aligned}$$

and system matrices defined as

$$\begin{aligned} A_{\text{dc}} &:= \text{blkdiag}(A_{\text{dc},1}, \dots, A_{\text{dc},M}), \\ B_{\text{dc}} &:= \text{blkdiag}(B_{\text{dc},1}, \dots, B_{\text{dc},M}), \\ B_{\text{dc}}^w &:= \text{blkdiag}(B_{\text{dc},1}^w, \dots, B_{\text{dc},M}^w). \end{aligned}$$

## 3.3 AC System Model

### 3.3.1 Modeling of a Single AC System $h$

The dynamic model of each AC system is represented by an aggregated generator and turbine-governor model, given by [37]

$$2\pi J_h \dot{f}_h = \frac{P_{\text{m},h} - P_{1,h} - P_{\text{dc},h}}{2\pi f_h} - 2\pi D_{\text{g},h}(f_h - f_{\text{nom},h}), \quad (3.6a)$$

$$T_{\text{m},h} \dot{P}_{\text{m},h} = P_{\text{m},h}^0 - P_{\text{m},h} - \frac{P_{\text{nom},h}}{\sigma_h} \frac{f_h - f_{\text{nom},h}}{f_{\text{nom},h}}, \quad (3.6b)$$

with  $P_{1,h}$  defined as:

$$P_{1,h} := P_{1,h}^0 (1 + D_{1,h}(f_h - f_{\text{nom},h})). \quad (3.6c)$$

It should be noted that we are only considering dynamics of system variables on a 2+ second time-scale. Equation (3.6a) is the swing equation representing the electro-mechanical dynamics of AC system  $h$ :

- $f_h(t)$  and  $f_{\text{nom},h}$  are, respectively, the frequency and the nominal frequency of the system in Hz.
- $J_h$  is the the moment of inertia of the aggregated area generator in  $\text{kg.m}^2$  and  $D_{\text{g},h}$  is its damping coefficient in  $\text{W.s}^2$ .

- $P_{m,h}(t)$  is the aggregated mechanical power in W.
- $P_{l,h}(t)$  is the aggregated power load in W which fluctuates with sensitivity factor  $D_{l,h}$  to frequency deviation. The nominal-frequency value  $P_{l,h}^0(t)$  in W can be viewed as an input of the consumers to the power network.
- $P_{dc,h}(t)$  is the total power injected by AC system  $h$  into the HVDC systems in W such that

$$P_{dc,h}(t) := \sum_{l \in \mathcal{N}_h} P_{vsc,l} = c_h^\top P_{vsc}, \quad (3.7)$$

where  $\mathcal{N}_h$  represents the set of HVDC systems connected to AC system  $h$  and  $c_h \in \mathbb{R}^{\Sigma^p}$  is defined in (3.1)

Equation (3.6b) represents the dynamics of local primary frequency control by the governor for AC system  $h$ :

- $T_{m,h}$  is the time constant for local power adjustment in seconds.
- $P_{m,h}^0(t)$ , in W, is set by secondary frequency control over a time scale that is greater than 30 seconds. Therefore,  $P_{m,h}^0(t)$  is considered a constant such that:  $P_{m,h}^0(t) = \bar{P}_{m,h}^0$ .
- $P_{nom,h}$  is the rated power of the aggregate generator of AC system  $h$  in W and  $\sigma_h$  is the governor droop.

We should stress on the fact that (3.6) is an aggregate model representing an entire AC area and is not a generator model. Hence, rotor angles are not modeled. Furthermore, it is implicitly assumed that the aggregated generators are not heavily loaded so that the Automatic Voltage Regulator (AVR) and exciter systems are not strongly activated.

Next, we define a reference operating point which is a particular equilibrium defined by specific values of input parameters and variables whereby the system is assumed to be at rest. We label system variables operating at the reference operating point with a bar. Denote by  $\bar{P}_{m,h}^0$  and  $\bar{P}_{l,h}^0$  the values of  $P_{m,h}^0$  and  $P_{l,h}^0$  at the reference operating point, respectively. We further assume that the value of the frequency at the reference operating point is equal to the nominal frequency for all systems such that

$$\bar{f}_h = f_{nom,h}, \quad \text{for } h = 1, \dots, N.$$

It follows from (3.6c) that

$$\bar{P}_{l,h} = \bar{P}_{l,h}^0, \quad \text{for } h = 1, \dots, N,$$

and from (3.6a) and (3.6b) that

$$\begin{aligned}\bar{P}_{m,h} &= \bar{P}_{m,h}^0, \quad \text{for } h = 1, \dots, N, \\ \bar{P}_{dc,h} &= \bar{P}_{m,h} - \bar{P}_{1,h} \\ &= \bar{P}_{m,h}^0 - \bar{P}_{1,h}^0, \quad \text{for } h = 1, \dots, N.\end{aligned}$$

It is evident that (3.6a)-(3.6c) introduce non-linearity to the AC system model. We define the following deviation variables:

$$\begin{aligned}\Delta f_h &:= f_h - \bar{f}_h = f_h - f_{\text{nom},h}, \\ \Delta P_{m,h} &:= P_{m,h} - \bar{P}_{m,h} = P_{m,h} - \bar{P}_{m,h}^0, \\ \Delta P_{1,h}^0 &:= P_{1,h}^0 - \bar{P}_{1,h}^0, \\ \Delta P_{dc,h} &:= P_{dc,h} - \bar{P}_{dc,h}, \\ \Delta P_{m,h}^0 &:= P_{m,h}^0 - \bar{P}_{m,h}^0 = \bar{P}_{m,h}^0 - \bar{P}_{m,h}^0 = 0.\end{aligned}$$

The standard linearization of (3.6a)-(3.6c) is derived in Appendix A.1 and is given by

$$J_h \Delta \dot{f}_h = \frac{\Delta P_{m,h} - \Delta P_{1,h}^0 - \Delta P_{dc,h}}{4\pi^2 f_{\text{nom},h}} - \left( D_{g,h} + \frac{\bar{P}_{1,h}^0 D_{1,h}}{4\pi^2 f_{\text{nom},h}} \right) \Delta f_h.$$

Rearranging and substituting (3.7), we get

$$(4\pi^2 f_{\text{nom},h}) J_h \Delta \dot{f}_h = \Delta P_{m,h} - \Delta P_{1,h}^0 - c_h^\top u - D_h \Delta f_h, \quad (3.8)$$

with  $D_h := (4\pi^2 f_{\text{nom},h}) D_{g,h} + \bar{P}_{1,h}^0 D_{1,h}$ .

Representing (3.6b) in deviation variables, we obtain

$$T_{m,h} \Delta \dot{P}_{m,h} = \Delta P_{m,h}^0 - \Delta P_{m,h} - \frac{P_{\text{nom},h}}{\sigma_h f_{\text{nom},h}} \Delta f_h. \quad (3.9)$$

$\Delta P_{m,h}^0$  in (3.9) is equal to zero since  $P_{m,h}^0(t)$  is considered a constant such that:  $P_{m,h}^0(t) = \bar{P}_{m,h}^0$ . Hence,  $\Delta P_{m,h}^0 = P_{m,h}^0 - \bar{P}_{m,h}^0 = 0$ . Therefore, (3.9) becomes

$$T_{m,h} \Delta \dot{P}_{m,h} = -\Delta P_{m,h} - \frac{P_{\text{nom},h}}{\sigma_h f_{\text{nom},h}} \Delta f_h. \quad (3.10)$$

### 3.3.2 Modeling of the Set of $N$ AC Systems

Representing (3.8) and (3.10) for  $N$  AC systems in matrix form, we get

$$\begin{aligned} J\Delta\dot{f} &= -D\Delta f - \mathcal{C}^\top u + \Delta P_m - \Delta P_1^0, \\ T_m\Delta\dot{P}_m &= -\Delta P_m - K\Delta f, \end{aligned}$$

where,

$$\begin{aligned} \mathcal{C} &:= [c_1 \ \dots \ c_N], \\ J &:= \text{diag}((4\pi^2 f_{\text{nom},1})J_1, \dots, (4\pi^2 f_{\text{nom},N})J_N), \\ D &:= \text{diag}(D_1, \dots, D_N), \\ T_m &:= \text{diag}(T_{m,1}, \dots, T_{m,N}), \\ K &:= \text{diag}\left(\frac{P_{\text{nom},1}}{\sigma_1 f_{\text{nom},1}}, \dots, \frac{P_{\text{nom},N}}{\sigma_N f_{\text{nom},N}}\right), \end{aligned}$$

and,

$$\begin{aligned} \Delta f &:= \text{col}(\Delta f_1, \dots, \Delta f_N), \\ \Delta P_1^0 &:= \text{col}(\Delta P_{1,1}^0, \dots, \Delta P_{1,N}^0), \\ \Delta P_m &:= \text{col}(\Delta P_{m,1}, \dots, \Delta P_{m,N}). \end{aligned}$$

The state space representation of the  $N$  AC systems becomes

$$\dot{x}_{\text{ac}} = A_{\text{ac}}x_{\text{ac}} + B_{\text{ac}}u + B_{\text{ac}}^w w_{\text{ac}},$$

with state, input, and disturbance vectors defined as

$$x_{\text{ac}} := \text{col}(\Delta f, \Delta P_m), \quad u := \text{col}(u_1, \dots, u_M), \quad w_{\text{ac}} := \Delta P_1^0,$$

and system matrices defined as

$$\begin{aligned} A_{\text{ac}} &:= \begin{bmatrix} -J^{-1}D & J^{-1} \\ -T_m^{-1}K & -T_m^{-1} \end{bmatrix}, \\ B_{\text{ac}} &:= \begin{bmatrix} -J^{-1}\mathcal{C}^\top \\ 0 \end{bmatrix}, \\ B_{\text{ac}}^w &:= \begin{bmatrix} -J^{-1} \\ 0 \end{bmatrix}. \end{aligned}$$

### 3.4 Overall System Model

Augmenting the DC and AC models into a single state space representation, we get a system of the form

$$\dot{x} = Ax + Bu + B_w w,$$

where the augmented system state, control input, and disturbance are defined as

$$x := \text{col}(x_{\text{dc}}, x_{\text{ac}}), \quad u := \text{col}(u_1, \dots, u_M), \quad w := \text{col}(w_{\text{dc}}, w_{\text{ac}}),$$

with system matrices defined as

$$A := \left[ \begin{array}{c|c} A_{\text{dc}} & \\ \hline & A_{\text{ac}} \end{array} \right],$$

$$B_w := \left[ \begin{array}{c|c} B_{\text{dc}}^w & \\ \hline & B_{\text{ac}}^w \end{array} \right],$$

$$B := \begin{bmatrix} B_{\text{dc}} \\ B_{\text{ac}} \end{bmatrix}.$$

## Chapter 4

# OSS Control in MTDC Systems

In this chapter, we apply the LC-OSS control framework to MTDC systems. In Section 4.1, we show that the LC-OSS control encompasses some of the existing MTDC controllers proposed in the literature. In Section 4.2, we state the control objectives to be achieved and define the convex optimization problem accordingly. In Section 4.3 we develop the OSS controller that should drive the system to to the the equilibrium corresponding to the optimal output which minimizes the optimization problem defined. In Section 4.4, we provide a simplified stability analysis of the closed-loop system.

### 4.1 Special Cases of LC-OSS Control in the Literature

In this section, we show that the LC-OSS control encompasses some of the existing MTDC controllers proposed in the literature. In particular, we show that the OSS controller recovers controllers that behave similar to the distributed power consensus controller proposed in [37], and to the decentralized voltage controller proposed in [38]. In addition, we study the stability of the closed-loop systems. We first start by laying down the modeling assumptions for which the controllers in this section will be applied to.

**Assumption 4.1.1.** The system is composed of one HVDC system consisting of  $n$  nodes, each node is connected to an AC system via a VSC.

**Assumption 4.1.2.** The HVDC voltage and current dynamics are neglected.

**Assumption 4.1.3.** The HVDC system is assumed to be lossless, i.e., the net power injected into the HVDC system should be equal to zero:  $\mathbf{1}^\top u = 0$ .

Hence, system dynamics are governed by the continuous-time LTI state-space model

$$\begin{aligned} \dot{x} &= Ax + Bu + B_w w, \\ y &= Cx + Du + D_w w, \end{aligned} \quad (4.1)$$

where the system state, control input, and disturbance are defined as

$$x := \text{col}(\Delta f, \Delta P_m) \in \mathbb{R}^{2n}, \quad u := \Delta P_{\text{vsc}} \in \mathbb{R}^n, \quad w := \Delta P_1^0 \in \mathbb{R}^n,$$

and system matrices are defined as

$$A := \begin{bmatrix} -J^{-1}D & J^{-1} \\ -T_m^{-1}K & -T_m^{-1} \end{bmatrix}, \quad B := \begin{bmatrix} -J^{-1} \\ 0 \end{bmatrix}, \quad B_w := \begin{bmatrix} -J^{-1} \\ 0 \end{bmatrix}.$$

The measured output variable is frequency deviation in AC systems, i.e.,  $y := \Delta f$ . Therefore,  $C$ ,  $D$ , and  $D_w$  are defined such that

$$C := [I \ 0], \quad D = 0, \quad D_w = 0.$$

It should be noted that the system (4.1) is internally exponentially stable, i.e.,  $A$  is Hurwitz. Therefore, the steady-state input-output mapping of (4.1) is

$$\bar{y} = G_u \bar{u} + G_w w,$$

where the DC gain matrices of (4.1) are defined as

$$\begin{aligned} G_u &:= -CA^{-1}B + D, \\ G_w &:= -CA^{-1}B_w + D_w. \end{aligned}$$

#### 4.1.1 Distributed Power Consensus Control

The control law proposed in [37] is motivated by the consensus algorithm, and is defined as a proportional-integral type controller at every VSC that requires a communication graph between the network nodes. The control law for VSC  $h$  is defined as

$$\Delta P_{\text{vsc},h} = \sum_{k=1}^n b_{hk} \left( \alpha \int (\Delta f_h - \Delta f_k) dt + \beta (\Delta f_h - \Delta f_k) \right), \quad (4.2)$$

where  $\alpha, \beta$  are positive gains and the coefficients  $b_{hk}$  model communication between AC areas;  $b_{hk} = 1$  if sub-controller  $h$  receives frequency information from area  $k$ , otherwise  $b_{hk} = 0$ . It is assumed that the communication graph is undirected, i.e.,  $b_{hk} = b_{kh}$  for all  $h, k = 1, \dots, n$ , and connected.

Rearranging (4.2) and differentiating both sides, we get

$$\Delta \dot{P}_{\text{vsc},h} = \alpha \left( \sum_{k=1}^n b_{hk} (\Delta f_h - \Delta f_k) \right) + \beta \left( \sum_{k=1}^n b_{hk} (\Delta \dot{f}_h - \Delta \dot{f}_k) \right). \quad (4.3)$$

Denoting (4.3) in matrix format, it could be written as

$$\Delta \dot{P}_{\text{vsc}} = \alpha \mathcal{L}_c (\Delta f) + \beta \mathcal{L}_c (\Delta \dot{f}),$$

where  $\mathcal{L}_c \in \mathbb{S}^n$  is the Laplacian matrix of the communication graph between the AC areas and is defined as

$$\mathcal{L}_c^{hk} := \begin{cases} -b_{hk}, & h \neq k \\ \sum_k b_{hk}, & h = k. \end{cases}$$

Denoting the control law in terms of input and output variables, we get

$$\dot{u} = \alpha \mathcal{L}_c y + \beta \mathcal{L}_c \dot{y}. \quad (4.4)$$

At equilibrium, we require the following conditions to hold:

$$\begin{aligned} A\bar{x} + B\bar{u} + B_w w &= 0, \\ \mathbf{1}^\top \bar{u} &= 0. \end{aligned}$$

A candidate matrix  $\mathcal{N}$  which satisfies the property  $\text{range}(\mathcal{N}) = \text{null} \underbrace{\begin{bmatrix} A & B \\ 0 & \mathbf{1}^\top \end{bmatrix}}_{:=\mathcal{K}}$  is

$$\mathcal{N} = \begin{bmatrix} -(D+K)^{-1} \mathcal{L}_c \\ K(D+K)^{-1} \mathcal{L}_c \\ \mathcal{L}_c \end{bmatrix}.$$

By substitution, one may verify that  $\text{range}(\mathcal{N}) \subseteq \text{null}(\mathcal{K})$ . Furthermore, by the construction of matrix  $\mathcal{K}$  we know that  $\text{nullity}(\mathcal{K}) = 2n - \text{rank}(\mathcal{K}) = 2n - (n+1) = n-1$ . Since  $\text{rank}(\mathcal{N}) = n-1$ , then  $\text{rank}(\mathcal{N}) = \text{nullity}(\mathcal{K})$  which implies that  $\text{range}(\mathcal{N}) = \text{null}(\mathcal{K})$ .

Next, we derive  $G_u$  defined such that  $G_u := [C \ D] \mathcal{N} = -(D+K)^{-1} \mathcal{L}_c$ .

The objective function associated to the LC-OSS controller is a quadratic convex cost

function in  $y$  defined as

$$f(y) = \frac{1}{2}y^\top Fy, \quad (4.5)$$

where  $F \in \mathbb{S}^n$  is a positive definite matrix.

The OSS problem then converts to a stabilization problem of the below augmented system

$$\begin{aligned} \dot{x} &= Ax + Bu + B_w w, \\ \tau \dot{\eta} &:= G_u^\top \nabla f(y) = -\mathcal{L}_c(D + K)^{-1} Fy, \end{aligned}$$

where  $\tau > 0$  is the *time-scale separation* time constant. Choosing  $F = D + K \succ 0$ , then the controller (4.6)

$$\tau \dot{\eta} = -\mathcal{L}_c y, \quad (4.6a)$$

$$u = -\alpha \eta + \beta \mathcal{L}_c y, \quad (4.6b)$$

recovers a distributed consensus controller that behaves similar to that proposed in [37]. The closed-loop system (4.1),(4.6) is stable as proved in Theorem 4.1.1.

**Theorem 4.1.1.** *There exists  $\beta^* > 0$  and  $\tau^* > 0$  such that the closed-loop system (4.1),(4.6) is stable for all  $\beta \in (0, \beta^*)$ ,  $\tau \in (\tau^*, +\infty)$ , and  $\alpha > 0$ .*

*Proof.* We define matrix  $\tilde{C} := \mathcal{L}_c C$  and  $\epsilon := 1/\tau$  such that the system (4.1) can be written as

$$\begin{aligned} \dot{x} &= Ax + Bu + B_w w, \\ \dot{\tilde{y}} &= \tilde{C}x, \end{aligned} \quad (4.7)$$

and the controller (4.6) can be written as

$$\begin{aligned} \dot{\eta} &= -\epsilon \tilde{y}, \\ u &= -\alpha \eta + \beta \tilde{y}. \end{aligned} \quad (4.8)$$

The closed-loop system becomes

$$\begin{bmatrix} \dot{x} \\ \dot{\eta} \end{bmatrix} = \begin{bmatrix} \tilde{A} & -\alpha B \\ -\epsilon \tilde{C} & 0 \end{bmatrix} \begin{bmatrix} x \\ \eta \end{bmatrix} + \begin{bmatrix} B_w \\ 0 \end{bmatrix} w,$$

where  $\tilde{A} := A + \beta B \tilde{C}$ . The expression  $A + \beta B \tilde{C}$  is a continuous function in  $\beta$  and is Hurwitz for  $\beta = 0$ . By continuity, there exists  $\beta^* > 0$  such that  $A + \beta B \tilde{C}$  is Hurwitz

for all  $\beta \in (0, \beta^*)$ .

Next, we introduce the change of variable  $\tilde{x} := x - \alpha \tilde{A}^{-1} B \eta$ . The closed-loop system becomes

$$\begin{bmatrix} \dot{\tilde{x}} \\ \dot{\eta} \end{bmatrix} = \underbrace{\begin{bmatrix} \tilde{A} + \epsilon M_1 & \epsilon M_2 \\ -\epsilon \tilde{C} & \epsilon G_\eta(0) \end{bmatrix}}_{:=\mathcal{A}} \begin{bmatrix} \tilde{x} \\ \eta \end{bmatrix} + \begin{bmatrix} B_w \\ 0 \end{bmatrix} w, \quad (4.9a)$$

where  $M_1 := \alpha \tilde{A}^{-1} B \tilde{C}$ ,  $M_2 := \alpha \tilde{A}^{-1} B \tilde{C} \tilde{A}^{-1} B$ , and

$$G_\eta(0) := \alpha \tilde{G}_\eta(0), \quad (4.9b)$$

$$\tilde{G}_\eta(0) := -\tilde{C} \tilde{A}^{-1} B = -\mathcal{L}_c(D + K + \beta \mathcal{L}_c)^{-1}. \quad (4.9c)$$

The second equality of (4.9c) is detailed in Appendix B.1.

By Theorem 2.3.4, since  $\tilde{A}$  is Hurwitz, then there exists  $P_1 \succ 0$  such that

$$Q_1 := \tilde{A}^\top P_1 + P_1 \tilde{A} \prec 0.$$

Moreover, since  $\alpha > 0$ ,  $\mathcal{L}_c \succeq 0$ , and  $(D + K + \beta \mathcal{L}_c)^{-1} \succ 0$ , then by Corollary 2.3.3,  $\sigma(G_\eta(0)) \in (-\infty, 0]$  with  $n_0(G_\eta(0)) = 1$ . Therefore, by Theorem 2.3.4 there exists  $P_2 \succ 0$  such that

$$Q_2 := G_\eta(0)^\top P_2 + P_2 G_\eta(0) \preceq 0.$$

Theorem 2.3.4 states that the system (4.9a) is stable if and only if there exists  $P \succ 0$  such that

$$\mathcal{Q} := \mathcal{A}^\top P + P \mathcal{A} \preceq 0.$$

We propose the matrix  $P \succ 0$  such that  $P := \text{blkdiag}(P_1, P_2)$  and compute the matrix  $\mathcal{Q}$  such that:

$$\begin{aligned} \mathcal{Q} &= \begin{bmatrix} (\tilde{A}^\top P_1 + P_1 \tilde{A}) + \epsilon(M_1^\top P_1 + P_1 M_1) & \epsilon(-\tilde{C}^\top P_2 + P_1 M_2) \\ \epsilon(M_2^\top P_1 - P_2 \tilde{C}) & \epsilon(G_\eta(0)^\top P_2 + P_2 G_\eta(0)) \end{bmatrix} \\ &= \begin{bmatrix} Q_1 + \epsilon R & \epsilon S \\ \epsilon S^\top & \epsilon Q_2 \end{bmatrix} \end{aligned}$$

with  $R := M_1^\top P_1 + P_1 M_1$  and  $S := -\tilde{C}^\top P_2 + P_1 M_2$ .

To prove that the closed-loop system is stable, we need the following lemma.

**Lemma 4.1.1.** *Given the real symmetric block matrix  $\mathcal{M}$*

$$\mathcal{M} = \begin{bmatrix} Q_1 + \epsilon R & \epsilon S \\ \epsilon S^\top & \epsilon Q_2 \end{bmatrix},$$

where  $Q_1 \prec 0$ ,  $Q_2 \preceq 0$ , and  $\epsilon > 0$ , then there exists  $\epsilon^* > 0$  such that  $\mathcal{M} \preceq 0$  for all  $\epsilon \in (0, \epsilon^*)$ .

*Proof.* The expression  $Q_1 + \epsilon R$  is a continuous function in  $\epsilon$  and is negative definite for  $\epsilon = 0$ . By continuity,  $Q_1 + \epsilon R \prec 0$  for sufficiently small  $\epsilon$ . By Theorem 2.3.5,  $\mathcal{M} \preceq 0$  if and only if

$$\epsilon Q_2 - \epsilon^2 S^\top (Q_1 + \epsilon R)^{-1} S \preceq 0,$$

which holds for  $\epsilon > 0$  if and only if

$$Q_2 - \epsilon S^\top (Q_1 + \epsilon R)^{-1} S \preceq 0.$$

Similarly, the expression  $Q_2 - \epsilon S^\top (Q_1 + \epsilon R)^{-1} S$  is a continuous function in  $\epsilon$  and is negative semi-definite for  $\epsilon = 0$ . By continuity, there exists  $\epsilon^* > 0$  such that  $Q_2 - \epsilon S^\top (Q_1 + \epsilon R)^{-1} S \preceq 0$  for all  $\epsilon \in (0, \epsilon^*)$  which completes the proof.  $\square$

Finally by applying Lemma 4.1.1 to  $\mathcal{Q}$ , we deduce that there exists  $\epsilon^* > 0$  such that  $\mathcal{Q} \preceq 0$  for all  $\epsilon \in (0, \epsilon^*)$ . Hence, we have  $P \succ 0$  and  $\mathcal{Q} \preceq 0$  that solves the Lyapunov equation  $\mathcal{Q} = \mathcal{A}^\top P + P\mathcal{A}$  for all  $\epsilon \in (0, \epsilon^*)$  and all  $\beta \in (0, \beta^*)$ .

Therefore, given  $\alpha > 0$ , there exists  $\beta^* > 0$  and  $\tau^* > 0$  such that the closed-loop system (4.1),(4.6) is stable for all  $\beta \in (0, \beta^*)$ ,  $\tau \in (\tau^*, +\infty)$ .  $\square$

The stability of the closed-loop system proved in Theorem 4.1.1 implies that  $\dot{\eta}(t) \rightarrow 0$  as  $t \rightarrow 0$  which is equivalent to the satisfying the KKT gradient condition at steady state by driving the optimality gap to zero. Hence, the cost function (4.5) is minimized at steady state.

## 4.1.2 Decentralized Voltage Control

In [37] and [38], a decentralized voltage control is applied to an MTDC network modeled as per Assumptions 4.1.1, 4.1.2, and 4.1.3. The control law proposed in the above papers is a proportional decentralized voltage controller defined as

$$v_h = \gamma \Delta f_h, \tag{4.10}$$

where  $\gamma \in \mathbb{R}$  is a positive constant.

By Ohm's law, the power injected into the HVDC network  $P_{\text{vsc},h}$  for  $h = 1, \dots, n$ , should satisfy:

$$P_{\text{vsc},h} = \sum_{k=1}^n \frac{V_h^{\text{dc}}}{R_{hk}} (V_h - V_k), \quad (4.11)$$

where,

$$\begin{aligned} V_h &= \bar{V}_h + v_h, \\ P_{\text{vsc},h} &= \bar{P}_{\text{vsc},h} + \Delta P_{\text{vsc},h}. \end{aligned}$$

The linearization of (4.11) is given by

$$\Delta P_{\text{vsc},h} = \frac{\bar{P}_{\text{vsc},h}}{\bar{V}_h} v_h + \sum_{k=1}^n \frac{\bar{V}_h}{R_{hk}} (v_h - v_k). \quad (4.12)$$

The matrix representation of (4.12) is

$$u = \Delta P_{\text{vsc}} = (\bar{V}^{-1} \bar{P} + \bar{V} \mathcal{L}_{\text{dc}}) v,$$

with  $\bar{P}$ ,  $\bar{V}$ , and  $v$  defined as

$$\begin{aligned} \bar{P} &:= \text{diag}(\bar{P}_{\text{vsc},1}, \dots, \bar{P}_{\text{vsc},n}), \\ \bar{V} &:= \text{diag}(\bar{V}_1, \dots, \bar{V}_n), \\ v &= \text{col}(v_1, \dots, v_n), \end{aligned}$$

and the connected weighted Laplacian matrix of the graph describing the HVDC grid  $\mathcal{L}_{\text{dc}}$  defined as

$$\mathcal{L}_{\text{dc}}^{hk} := \begin{cases} -\frac{1}{R_{hk}}, & h \neq k, \\ \sum_k \frac{1}{R_{hk}}, & h = k. \end{cases}$$

Defining the output vector  $y = \text{col}(\Delta f, u)$ , the corresponding  $C$ ,  $D$ , and  $D_w$  matrices are given by

$$C = \begin{bmatrix} I & 0 \\ 0 & 0 \end{bmatrix}, \quad D = \begin{bmatrix} 0 \\ I \end{bmatrix}, \quad D_w = \begin{bmatrix} 0 \\ 0 \end{bmatrix}.$$

Similar to the derivation in the previous section, a candidate  $G_u$  is given by

$$G_u := \begin{bmatrix} -(D + K)^{-1} \mathcal{L}_{\text{dc}} \\ \mathcal{L}_{\text{dc}} \end{bmatrix}.$$

Next, we define a cost function that minimizes  $v_h - \gamma \Delta f_h$  in order to achieve the decentralized voltage controller (4.10) by driving  $v_h$  to be equal to  $\gamma \Delta f_h$ . A candidate quadratic cost function is

$$f(v, \Delta f) = (v - \gamma \Delta f)^\top (v - \gamma \Delta f), \quad (4.13)$$

where  $\Delta f = \text{col}(\Delta f_1, \dots, \Delta f_n)$ .

In order to express  $v$  in terms of  $u$ , we need the following assumption:

**Assumption 4.1.4.**  $(\bar{V}^{-1} \bar{P} + \bar{V} \mathcal{L}_{\text{dc}})$  is a non-singular matrix with  $\sum_{i=1}^n \bar{P}_{\text{vsc},i} / \bar{V}_i^2 \neq 0$ .

Assumption 4.1.4 is a plausible assumption by the following logic. We will study the matrix  $\tilde{M} := (\bar{P} + \bar{V} \mathcal{L}_{\text{dc}} \bar{V})$  as its invertibility property is equivalent to that of  $(\bar{V}^{-1} \bar{P} + \bar{V} \mathcal{L}_{\text{dc}})$ . It is evident that  $\bar{V} \mathcal{L}_{\text{dc}} \bar{V}$  is positive semi-definite with  $\text{null}(\bar{V} \mathcal{L}_{\text{dc}} \bar{V})$  spanned by  $\alpha \bar{V}^{-1} \mathbf{1}$  where  $\alpha \in \mathbb{R}$ . Moreover, since  $\bar{V} \mathcal{L}_{\text{dc}} \bar{V}$  is orders of magnitude greater than  $\bar{P}$ , the eigenvalues of  $\bar{P}$  do not significantly perturb the positive eigenvalues of  $\bar{V} \mathcal{L}_{\text{dc}} \bar{V}$ .<sup>1</sup> Hence, we are only concerned about the perturbation of the zero eigenvalue of  $\bar{V} \mathcal{L}_{\text{dc}} \bar{V}$ . If we left and right multiply  $\tilde{M}$  by  $\alpha \mathbf{1}^\top \bar{V}^{-1}$  and  $\alpha \bar{V}^{-1} \mathbf{1}$  respectively, we get

$$\alpha^2 (\mathbf{1}^\top \bar{V}^{-1}) \tilde{M} (\bar{V}^{-1} \mathbf{1}) = \alpha^2 \mathbf{1}^\top \bar{V}^{-1} \bar{P} \bar{V}^{-1} \mathbf{1} = \alpha^2 \sum_{i=1}^n \bar{P}_{\text{vsc},i} / \bar{V}_i^2.$$

Assuming that  $\sum_{i=1}^n \bar{P}_{\text{vsc},i} / \bar{V}_i^2 \neq 0$ , then the zero eigenvalue of  $\bar{V} \mathcal{L}_{\text{dc}} \bar{V}$  is perturbed away from zero and consequently  $\tilde{M}$  does not possess zero eigenvalues. Therefore,  $\tilde{M}$  is non-singular matrix. In the remaining body of this section, we will adopt Assumption 4.1.4 such that  $v = Mu$  where  $M := (\bar{V}^{-1} \bar{P} + \bar{V} \mathcal{L}_{\text{dc}})^{-1}$ .

Hence, (4.13) can be written in terms of the output variable  $y$  as

$$f(y) = y^\top \underbrace{\begin{bmatrix} M^2 & -\gamma M^\top \\ -\gamma M & \gamma^2 I \end{bmatrix}}_{:=\mathcal{F}} y. \quad (4.14)$$

It should be noted that  $\mathcal{F} \succeq 0$ ; for  $v \in \mathbb{R}^{2n} \setminus \mathbb{0}$  such that  $v = \text{col}(v_1, v_2)$ ,  $v^\top \mathcal{F} v = \|Mv_1 - \gamma v_2\|_2^2 \geq 0$ . Hence,  $f(y)$  is a convex function in  $y$ .

<sup>1</sup>By the assumption that the nominal DC voltages  $\bar{V}_1, \dots, \bar{V}_n$  are in the range of 400 kV and the nominal VSC DC power  $\bar{P}_{\text{vsc},1}, \dots, \bar{P}_{\text{vsc},n}$  are in the range of 800 MW.

**Remark 4.1.1.** The controllers proposed in [37] and [38] are inherently inverse-optimal with respect to some objective. Hence, the implicitly minimized cost functions (4.5) and (4.14) do not have a physical meaning.

Choosing the low-gain integral controller,

$$\begin{aligned}\tau\dot{\eta} &= -G_u^\top \nabla f(y) = -\mathcal{L}_{\text{dc}} \begin{bmatrix} -(D+K)^{-1} & I \end{bmatrix} \mathcal{F}y, \\ u &= \eta,\end{aligned}\tag{4.15}$$

where  $\tau > 0$  is the time-scale separation time constant, would recover a decentralized voltage controller that behaves similar to that proposed in [37] and [38]. It is still left to prove that the proposed controller (4.15) stabilizes the closed-loop system.

**Theorem 4.1.2.** *There exists  $\tau^* > 0$  and  $\gamma^* > 0$  such that the closed-loop system (4.1),(4.15) is stable for all  $\tau \in (\tau^*, +\infty)$  and  $\gamma \in (0, \gamma^*)$ .*

*Proof.* With the feedback controller (4.15), the closed loop system is derived as

$$\begin{aligned}\dot{x} &= Ax + B\eta + B_w w, \\ y &= Cx + D\eta.\end{aligned}$$

and

$$\begin{aligned}\dot{\eta} &= -\epsilon \mathcal{L}_{\text{dc}} \begin{bmatrix} -(D+K)^{-1} & I \end{bmatrix} \mathcal{F}y, \\ &= -\epsilon \mathcal{L}_{\text{dc}} \begin{bmatrix} -(D+K)^{-1} & I \end{bmatrix} \mathcal{F}(Cx + D\eta), \\ &= -\epsilon \tilde{C}x - \epsilon \tilde{D}\eta\end{aligned}$$

where  $\tilde{C} := \mathcal{L}_{\text{dc}} \begin{bmatrix} -\Sigma & I \end{bmatrix} \mathcal{F}C$ ,  $\tilde{D} := \mathcal{L}_{\text{dc}} \begin{bmatrix} -\Sigma & I \end{bmatrix} \mathcal{F}D$ ,  $\Sigma := (D+K)^{-1}$ , and  $\epsilon := 1/\tau$ .

Next, we introduce the change of variable  $\tilde{x} := x + A^{-1}B\eta$ . The closed-loop system becomes

$$\begin{bmatrix} \dot{\tilde{x}} \\ \dot{\eta} \end{bmatrix} = \underbrace{\begin{bmatrix} A + \epsilon M_1 & \epsilon M_2 \\ -\epsilon \tilde{C} & \epsilon M_3 \end{bmatrix}}_A \begin{bmatrix} \tilde{x} \\ \eta \end{bmatrix} + \begin{bmatrix} B_w \\ \mathbb{0} \end{bmatrix} w,$$

where  $M_1 := -A^{-1}B\tilde{C}$ ,  $M_2 := A^{-1}B(\tilde{C}A^{-1}B - \tilde{D})$ , and  $M_3 := \tilde{C}A^{-1}B - \tilde{D}$ .

First, we derive the expression of  $\hat{M}_3 := \tilde{C}A^{-1}B$  such that

$$\hat{M}_3 = \tilde{C}A^{-1}B = -\mathcal{L}_{\text{dc}} \begin{bmatrix} -\Sigma & I \end{bmatrix} \mathcal{F} \underbrace{(-CA^{-1}B)}_{:=\tilde{G}(0)}.\tag{4.16}$$

It should be noted that  $\tilde{G}(0)$  is the dc gain matrix that maps  $u$  to  $\text{col}(\Delta f, \mathbb{0})$  and is

derived as  $\tilde{G}(0) = \text{col}(-\Sigma, 0)$ . Substituting in (4.16), we get

$$\hat{M}_3 = -\mathcal{L}_{\text{dc}}\left((M\Sigma)^\top(M\Sigma) + \gamma M\Sigma\right).$$

Expanding the expression of  $\tilde{D}$ , we obtain

$$\tilde{D} = \mathcal{L}_{\text{dc}}\left[-\Sigma \quad I\right] \mathcal{F}\left[0 \quad I\right]^\top = \mathcal{L}_{\text{dc}}(\gamma\Sigma M^\top + \gamma^2 I).$$

Hence,  $M_3$  simplifies to

$$M_3 = \hat{M}_3 - \tilde{D} = -\mathcal{L}_{\text{dc}}\left(\underbrace{(M\Sigma)^\top(M\Sigma) + \gamma(M\Sigma + \Sigma M^\top) + \gamma^2 I}_{\mathcal{M}}\right).$$

We know that  $\text{null}(M\Sigma) = \emptyset$  since  $\det(M\Sigma) = \det(M)\det(\Sigma) \neq 0$ . Therefore,  $(M\Sigma)^\top(M\Sigma) \succ 0$ . Moreover,  $\mathcal{M}$  is a continuous function in  $\gamma$  and is positive definite for  $\gamma = 0$ . By continuity, there exists  $\gamma^* > 0$  such that  $\mathcal{M} \succ 0$  for all  $\gamma \in (0, \gamma^*)$ . By Corollary 2.3.3,  $\sigma(M_3) \in (-\infty, 0]$  with  $n_0(M_3) = 1$ .

By Theorem 2.3.4:

- since  $A$  is Hurwitz, then there exists  $P_1 \succ 0$  such that  $Q_1 := A^\top P_1 + P_1 A \prec 0$ , and
- since  $\sigma(M_3) \in (-\infty, 0]$  with  $n_0(M_3) = 1$ , then there exists  $P_2 \succ 0$  such that  $Q_2 := M_3^\top P_2 + P_2 M_3 \preceq 0$ .

The remainder of the proof follows similar to that of Theorem 4.1.1.  $\square$

The stability of the closed-loop system proved in Theorem 4.1.2 implies that  $\dot{\eta}(t) \rightarrow 0$  as  $t \rightarrow \infty$  which is equivalent to the satisfying the KKT gradient condition at steady state by driving the optimality gap to zero. Hence, the cost function (4.13) is minimized at steady state and the decentralized controller (4.10) is recovered by the OSS framework.

## 4.2 OSS Problem Formulation

In this section, we define the convex optimization problem that the LC-OSS should minimize. Consider the problem

$$\underset{\bar{y}}{\text{minimize}} \quad f(\bar{y}) \tag{4.17a}$$

$$\text{subject to} \quad \bar{y} = G_u \bar{u} + G_w w, \tag{4.17b}$$

$$\mathcal{H}\bar{y} \leq h, \tag{4.17c}$$

where  $f(\bar{y})$  is a convex objective function to be minimized. The constraint (4.17b) is the steady-state constraint imposed by the dynamic system where  $G_u$  and  $G_w$  are the DC gain matrices of the system, and (4.17c) represents the set of soft engineering inequality constraints determined by  $\mathcal{H}$  and  $h$ .

We need to define the convex optimization problem (4.17) such that it achieves the following control objectives:

1. minimize the total power loss in HVDC systems,
2. minimize the frequency deviation in AC systems subject to unmeasured disturbance (load/generation changes), and
3. set upper and lower limits on HVDC link currents.

**Remark 4.2.1.** The identified control objectives cannot be met all at once; the closer we are to achieving one objective, the further we are from achieving the other one.

The measured outputs needed for achieving the above objectives are the HVDC line currents  $i_L$  and AC systems' frequency  $\Delta f$  which are defined as

$$\begin{aligned} i_L &:= \text{col}(i_{L,1}, \dots, i_{L,M}), \\ \Delta f &:= \text{col}(\Delta f_1, \dots, \Delta f_N). \end{aligned}$$

With the measured output signal  $y$  to be defined as  $y = \text{col}(i_L, \Delta f)$ , the cost function  $f(y)$  is given by

$$f(y) := \alpha_p f_p(y) + \alpha_f f_f(y) + \alpha_i f_i(y), \quad (4.18)$$

where  $f_p(y)$  is a penalty function on the total power loss in the HVDC systems,  $f_f(y)$  is a penalty function on frequency variations in AC systems, and  $f_i(y)$  is a penalty function on HVDC currents violations enforcing the soft inequality constraints (4.17c). The constants  $\alpha_p$ ,  $\alpha_f$ , and  $\alpha_i \in \mathbb{R}$  are positive scaling coefficients.

**Remark 4.2.2.** It is derived in Appendix B.2 that  $\mathbb{1}^\top \bar{u}_l = 0$  for  $l = 1, \dots, M$ , i.e, the sum of power injected through the VSCs into each HVDC system should be equal to zero. This implies that the model neglects the power loss in the HVDC system. This property is a direct consequence of Assumption 3.2.2.

Although the system's model neglects the power loss in HVDC systems as per Remark 4.2.2, the cost function penalizes physical power loss in these systems with  $f_p(y)$ . The

power loss in a single line  $i$  in HVDC system  $l$  is given by

$$\begin{aligned} P_{\text{loss},l}^i &= R_l^i (I_{L,l}^i)^2 \\ &= R_l^i (\bar{I}_{L,l}^i + i_{L,l}^i)^2 \\ &= \underbrace{R_l^i (\bar{I}_{L,l}^i)^2}_{:= \bar{P}_{\text{loss},l}^i} + \underbrace{2R_l^i \bar{I}_{L,l}^i i_{L,l}^i + R_l^i (i_{L,l}^i)^2}_{:= \Delta P_{\text{loss},l}^i}, \end{aligned}$$

where steady state variables are marked with a bar.

Then, the variation of the total power loss in HVDC system  $l$  is

$$\Delta P_{\text{loss},l} = i_{L,l}^\top R_l i_{L,l} + m_l^\top i_{L,l},$$

where  $m_l := 2R_l \bar{I}_{L,l}$ .

Finally, the total variation in power loss in all HVDC systems  $l = 1, \dots, M$  is expressed as

$$\Delta P_{\text{loss}} = i_L^\top M_p i_L + m^\top i_L,$$

where  $M_p = \text{blkdiag}(R_1, \dots, R_M)$  and  $m = \text{col}(m_1, \dots, m_M)$ .

Hence, the penalty function on the total power loss  $f_p(y)$  is defined as

$$f_p(y) := i_L^\top M_p i_L + m^\top i_L.$$

Next, we define a quadratic cost function on frequency variations in AC systems  $f_f(y)$  such that

$$f_f(y) := \Delta f^\top M_f \Delta f,$$

where  $M_f$  is a diagonal cost matrix.

Finally, we require the DC line currents to satisfy the following set of inequality constraints for  $k = 1, \dots, m_{\text{dc},l}$  and  $l = 1, \dots, M$ :

$$\bar{I}_{L,l}^k + i_{L,l}^k \geq I_{L,l}^{\min}, \quad (4.19a)$$

$$\bar{I}_{L,l}^k + i_{L,l}^k \leq I_{L,l}^{\max}, \quad (4.19b)$$

where  $I_{L,l}^{\min}$  and  $I_{L,l}^{\max}$  are the minimum and maximum acceptable current limits for lines of HVDC system  $l$ .

One approximate way to enforce the soft inequality constraints (4.19) is by defining

$f_i(y)$  such that

$$f_i(y) := P(i_L) := \sum_{l=1}^M \left( \sum_{k=1}^{m_{dc,l}} \max\left(0, I_{L,l}^{\min} - (\bar{I}_{L,l}^k + i_{L,l}^k), (\bar{I}_{L,l}^k + i_{L,l}^k) - I_{L,l}^{\max}\right)^2 \right).$$

### 4.3 LC-OSS HVDC Controller

In this section, we develop the OSS controller that will drive the system to the equilibrium  $(\bar{x}, \bar{u})$  corresponding to the optimal point  $\bar{y}^*$  of the problem (4.17). As derived in Appendix B.2, the steady state DC voltage and current for HVDC system  $l$  are given by

$$\bar{v}_{dc,l} = \frac{1}{V_{dc,l}^{\text{nom}}} \mathcal{L}_{dc,l}^\dagger \begin{bmatrix} I_{p_l} \\ 0 \end{bmatrix} \bar{u}_l + \beta_l \mathbf{1} + \tilde{v}_{dc,l}, \quad (4.20a)$$

$$\bar{i}_{L,l} = R_l^{-1} F_{dc,l}^\top \left( \frac{1}{V_{dc,l}^{\text{nom}}} \mathcal{L}_{dc,l}^\dagger \begin{bmatrix} I_{p_l} \\ 0 \end{bmatrix} \bar{u}_l + \beta_l \mathbf{1} \right) + \tilde{i}_{L,l}, \quad (4.20b)$$

where  $\mathcal{L}_{dc,l}$  for  $l = 1, \dots, M$  is the weighted Laplacian matrix of the graph describing HVDC grid  $l$  which is defined as  $\mathcal{L}_{dc,l} := F_{dc,l} R_l^{-1} F_{dc,l}^\top$ , and  $\tilde{v}_{dc,l}$  and  $\beta_l \in \mathbb{R}$  is a free variable. The vectors  $\tilde{v}_{dc,l}$  and  $\tilde{i}_{L,l}$  are constant disturbance vectors due to the constant DC disturbance  $w_{dc}$ .

Hence, according to (4.20b),  $\bar{i}_L$  can be written as:

$$\bar{i}_L = \hat{K} \bar{u} + \hat{i}_L,$$

where  $\hat{i}_L$  and  $\hat{K}$  are given by

$$\hat{i}_L := \text{col}\left((\beta_1 R_1^{-1} F_{dc,1}^\top \mathbf{1} + \tilde{i}_{L,1}), \dots, (\beta_M R_M^{-1} F_{dc,M}^\top \mathbf{1} + \tilde{i}_{L,M})\right),$$

$$\hat{K} := \text{blkdiag}\left(\frac{1}{V_{dc,1}^{\text{nom}}} R_1^{-1} F_{dc,1}^\top \mathcal{L}_{dc,1}^\dagger \begin{bmatrix} I_{p_1} \\ 0 \end{bmatrix}, \dots, \frac{1}{V_{dc,M}^{\text{nom}}} R_M^{-1} F_{dc,M}^\top \mathcal{L}_{dc,M}^\dagger \begin{bmatrix} I_{p_M} \\ 0 \end{bmatrix}\right).$$

We define the gain matrix  $\hat{G}_f$  that maps the steady state input  $\bar{u}$  to the steady state frequency deviation  $\Delta \bar{f}$  such that:

$$\Delta \bar{f} = \hat{G}_f \bar{u} + \Delta \hat{f},$$

$$\hat{G}_f := -C_{ac} A_{ac}^{-1} B_{ac} + D_{ac},$$

where  $\Delta \hat{f}$  is the steady state frequency deviation imposed by the constant disturbance  $w_{ac}$ . Matrices  $C_{ac}$  and  $D_{ac}$  are defined such that the measured AC output variable is  $\Delta f$ .

With  $y$  defined as  $y = \text{col}(i_L, \Delta f)$ , the dc gain matrix  $G_u$  is represented by

$$G_u := \begin{bmatrix} \hat{K} \\ \hat{G}_f \end{bmatrix},$$

such that

$$\bar{y} = G_u \bar{u} + \hat{y}, \quad (4.21)$$

where  $\hat{y}$  is a constant disturbance vector.

By Remark 4.2.2, we have  $p_l - 1$  independent control inputs for each of the HVDC systems. Hence, for each of the HVDC systems, the first  $p_l - 1$  control inputs will be controlled independently with  $p_l^{\text{th}}$  control input being the negative sum of remaining inputs which insures zero net power injected into the HVDC system.

Algebraically, we define  $\bar{u}_c \in \mathbb{R}^{p-M}$ , where  $p := \sum_{l=1}^M p_l$ , to be the first  $p_l - 1$  independently controlled inputs such that

$$\bar{u} := S \bar{u}_c,$$

where  $S \in \mathbb{R}^{p \times (p-M)}$  is the matrix that ensures power balance in each HVDC system. Matrix  $S$  is defined such that the  $p_l^{\text{th}}$  control input of HVDC system  $l$  is the negative sum of the independent control inputs and is given by

$$S := \text{blkdiag}(S_1, \dots, S_M)$$

$$S_l := \begin{bmatrix} I_{p_l-1} \\ -\mathbf{1}_{p_l-1}^\top \end{bmatrix}, \quad l = 1, \dots, M.$$

Therefore, (4.21) becomes  $\bar{y} = (G_u S) \bar{u}_c + \hat{y}$ .

Transforming the above optimization problem to a stabilization problem via the LC-OSS framework, we get the controller

$$\tau \dot{\eta} = -(G_u S)^\top \nabla f(\bar{y}), \quad (4.22a)$$

$$\bar{u}_c = \eta, \quad (4.22b)$$

$$\bar{u} = S \bar{u}_c. \quad (4.22c)$$

The gradient of the proposed cost function is given by

$$\begin{aligned}\nabla f(y) &= \text{col} \left( \frac{\partial f(y)}{\partial i_{\mathbf{L}}}, \frac{\partial f(y)}{\partial \Delta f} \right) \\ &= My + \text{col} \left( \alpha_{\text{p}} m + \nabla P(i_{\mathbf{L}}), \mathbf{0}_{n_{\text{ac}}} \right),\end{aligned}$$

where  $M := \text{blkdiag}(2\alpha_{\text{p}}M_{\text{p}}, 2\alpha_{\text{f}}M_{\text{f}})$  and the gradient of the current violation penalty function  $\nabla P(i_{\mathbf{L}})$  is defined as

$$\nabla P(i_{\mathbf{L}}) := \alpha_{\text{i}} \left( \text{col}(\nabla P(i_{\mathbf{L},1}), \dots, \nabla P(i_{\mathbf{L},M})) \right),$$

such that  $\nabla P(i_{\mathbf{L},l})$  for  $l = 1, \dots, M$  is defined as

$$\nabla P(i_{\mathbf{L},l}) := \text{col} \left( \frac{\partial P(i_{\mathbf{L}})}{\partial i_{\mathbf{L},l}^1}, \dots, \frac{\partial P(i_{\mathbf{L}})}{\partial i_{\mathbf{L},l}^{m_{\text{dc},l}}} \right),$$

and  $\frac{\partial P(i_{\mathbf{L}})}{\partial i_{\mathbf{L},l}^k}$  for  $k = 1, \dots, m_{\text{dc},l}$  is defined as

$$\frac{\partial P(i_{\mathbf{L}})}{\partial i_{\mathbf{L},l}^k} := \begin{cases} 2 \left( i_{\mathbf{L},l}^k - (I_L^{\min} - \bar{I}_{\mathbf{L},l}^k) \right), & i_{\mathbf{L},l}^k \in \left( -\infty, (I_L^{\min} - \bar{I}_{\mathbf{L},l}^k) \right), \\ 0, & i_{\mathbf{L},l}^k \in \left[ (I_L^{\min} - \bar{I}_{\mathbf{L},l}^k), (I_L^{\max} - \bar{I}_{\mathbf{L},l}^k) \right], \\ 2 \left( i_{\mathbf{L},l}^k - (I_L^{\max} - \bar{I}_{\mathbf{L},l}^k) \right), & i_{\mathbf{L},l}^k \in \left( (I_L^{\max} - \bar{I}_{\mathbf{L},l}^k), +\infty \right). \end{cases}$$

#### 4.4 Stability Analysis of the Proposed Controller

The block diagram of the controller is represented in Figure 4.1.

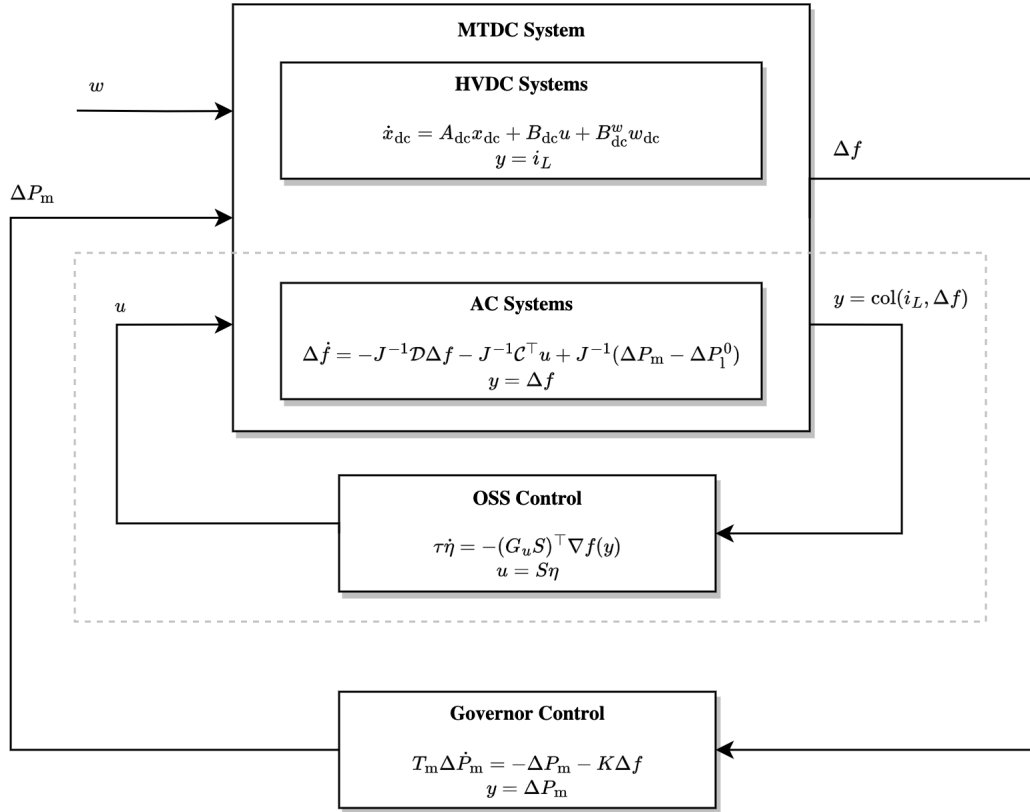


Figure 4.1: Block diagram of the MTDC-OSS controller

The intuition behind the controller design is as follows: the OSS controller dispatches power transfer commands to the VSCs before the governors of the AC systems take action. By that, the governors now respond to a power load variation that has been *reduced/adjusted* by the faster OSS control resulting in primary frequency reserve sharing between AC systems in addition to other set of objectives to be simultaneously met as identified in the previous section.

It should be noted that our system model can be divided onto three time scales:

1. a fast time scale for the HVDC voltage and current dynamics,
2. a slower time scale for the frequency and controller dynamics, and
3. a slow time time scale for the governor dynamics responding to power load variation in AC systems.

Since the HVDC systems' dynamics are orders of magnitude faster than that of the frequency and controller dynamics, the power transferred by the VSCs and injected into the HVDC systems changes very slowly as compared to the fast DC dynamics. Hence, the OSS controller output  $u$  is seen as a constant disturbance by the HVDC

systems and the internal stability of the HVDC systems is not affected by the OSS controller. Therefore, this section does not study the effect of the OSS controller on the stability of the HVDC systems. Moreover, the dynamics of the governor control is approximately 10 times slower than AC systems' frequency, therefore, the output of the governor control  $\Delta P_m$  is seen as a constant disturbance by the AC systems which does not affect its internal stability.

By the notion of time-scale separation described above, proving that the OSS controller preserves the stability of the AC systems is equivalent to proving that the whole system is stable. In this section we present a simplified stability analysis of the inner closed-loop system described by the swing equation of the AC systems and the OSS controller as highlighted in the dotted frame in Figure 4.1. We simplify the stability analysis by dropping the cost function components  $\alpha_i f_i(y)$  and  $\alpha_p f_p(y)$  such that  $f(y) = \alpha_f f_f(y)$ . The block diagram of the system for which we will analyze its stability is represented in Figure 4.2.

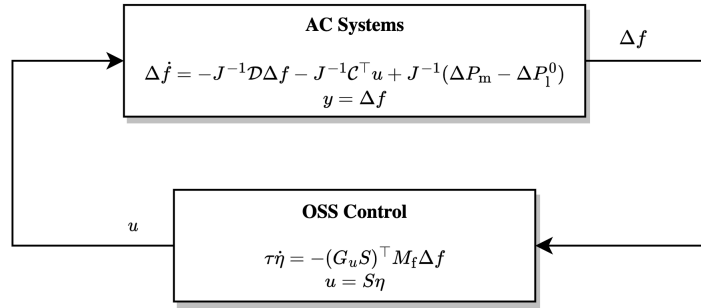


Figure 4.2: Block diagram of inner loop

The closed-loop system of the inner loop is given by

$$\begin{bmatrix} \dot{x} \\ \dot{\eta} \end{bmatrix} = \underbrace{\begin{bmatrix} A & BS \\ -\epsilon(G_u S)^\top \tilde{M}_f & 0 \end{bmatrix}}_{A_{CL}} \begin{bmatrix} x \\ \eta \end{bmatrix} + \underbrace{\begin{bmatrix} B_w \\ 0 \end{bmatrix}}_{B_{CL}^w} w \quad (4.23)$$

where  $\epsilon := 1/\tau$  and

$$\begin{aligned} A &:= -J^{-1} D, \\ B &:= -J^{-1} \mathcal{C}^\top, \\ B_w &:= J^{-1}, \\ \tilde{M}_f &:= 2\alpha_f M_f, \\ x &:= \Delta f, \\ w &:= \Delta P_m - \Delta P_1^0. \end{aligned}$$

The DC gain matrix of the swing equation,  $G_u$ , is defined such that  $G_u = -CA^{-1}B = -(I)(-J^{-1}D)^{-1}(-J^{-1}C^\top) = -D^{-1}C^\top$ .

For the stability of the closed-loop system in Figure 4.2, we prove the following theorem.

**Theorem 4.4.1.** *There exists  $\epsilon^* > 0$  such that the closed-loop system (4.23) is exponentially stable for all  $\epsilon \in (0, \epsilon^*)$ .*

*Proof.* With  $\tilde{C} := S^\top C D^{-1} \tilde{M}_f$  and  $\tilde{B} := B S$  the closed-loop system can be written as

$$\begin{bmatrix} \dot{x} \\ \dot{\eta} \end{bmatrix} = \begin{bmatrix} A & \tilde{B} \\ \epsilon \tilde{C} & 0 \end{bmatrix} \begin{bmatrix} x \\ \eta \end{bmatrix} + B_{\text{CL}}^w w$$

Next, we introduce the change of variable  $\tilde{x} := x + A^{-1} \tilde{B} \eta$ . The closed-loop system becomes

$$\begin{bmatrix} \dot{\tilde{x}} \\ \dot{\eta} \end{bmatrix} = \underbrace{\begin{bmatrix} A + \epsilon M_1 & \epsilon M_2 \\ \epsilon \tilde{C} & \epsilon M_3 \end{bmatrix}}_{:=A} \begin{bmatrix} \tilde{x} \\ \eta \end{bmatrix} + B_{\text{CL}}^w w,$$

where  $M_1$ ,  $M_2$ , and  $M_3$  are derived such that

$$M_1 := A^{-1} \tilde{B} \tilde{C}, \quad (4.24a)$$

$$M_2 := -A^{-1} \tilde{B} \tilde{C} A^{-1} \tilde{B}, \quad (4.24b)$$

$$M_3 := -\tilde{C} A^{-1} \tilde{B}. \quad (4.24c)$$

Substituting the expressions of  $A$ ,  $\tilde{B}$ , and  $\tilde{C}$  in (4.24c), we get:

$$\begin{aligned} M_3 &= -\tilde{C} A^{-1} \tilde{B} \\ &= -(S^\top C D^{-1} \tilde{M}_f)(-J^{-1} D)^{-1}(-J^{-1} C^\top S) \\ &= -(D^{-1} C^\top S)^\top \tilde{M}_f (D^{-1} C^\top S) \preceq 0 \end{aligned}$$

In order to obtain a closed-loop system that is exponentially stable, we require the following assumption on the topology of the interconnection between the HVDC and AC systems.

**Assumption 4.4.1.** The interconnection between the HVDC systems and AC systems, i.e., the choice of  $\mathcal{C}$ , is assumed to give  $\text{rank}(C^\top S) = N$ .

A sufficient connectivity condition for satisfying Assumption 4.4.1 is when we restrict the AC systems to be connected to only one HVDC system, i.e., an AC system cannot

be connected to multiple HVDC systems.

By Assumption 4.4.1, we get that  $\text{rank}(D^{-1}\mathcal{C}^\top S) = \text{rank}(\mathcal{C}^\top S) = N$ . Consequently,  $\text{null}(D^{-1}\mathcal{C}^\top S) = \emptyset$  and  $M_3 \prec 0$ .

Now, applying Lyapunov arguments to  $A$  and  $M_3$ , we get by Theorem 2.3.4 the following:

- since  $A$  is Hurwitz, then there exists  $P_1 \succ 0$  such that  $Q_1 := A^\top P_1 + P_1 A \prec 0$ , and
- since  $M_3$  is Hurwitz, then there exists  $P_2 \succ 0$  such that  $Q_2 := M_3^\top P_2 + P_2 M_3 \prec 0$ .

The remainder of the proof follows similar to that of Theorem 4.1.1 with one difference:  $Q \prec 0$  which implies that the inner loop is exponentially stable.  $\square$

**Remark 4.4.1.** It should be noted that the inner loop would be stable if we release Assumption 4.4.1 such that  $\text{rank}(\mathcal{C}^\top S) = N - 1$ , however, further analysis on the effect of the governor control on the zero eigenvalue is required for the stability of the full system.

## Chapter 5

# Simulation Results

In this chapter, we apply the controller (4.22) on an MTDC test system comprising of two HVDC systems connecting six AC systems. In Section 5.1, we introduce the overall test system topology, parameters, and operating point. In Section 5.2, we consider three different tunings of the controller to illustrate the options and flexibility inherent in the control scheme. In Section 5.3, we evaluate the controller's performance based on a time-domain simulation in MATLAB/Simulink environment in response to power load variations in four of the AC systems. Simulation results verify theoretical expectations as the controller is able to drive the system to the equilibrium corresponding to the optimizer of the different optimization problems applied.

### 5.1 Test System

The test system is comprised of eight interconnected systems; two HVDC systems and six AC systems as depicted in Figure 5.1. For both HVDC test systems, four VSC nodes connect DC to AC terminals.

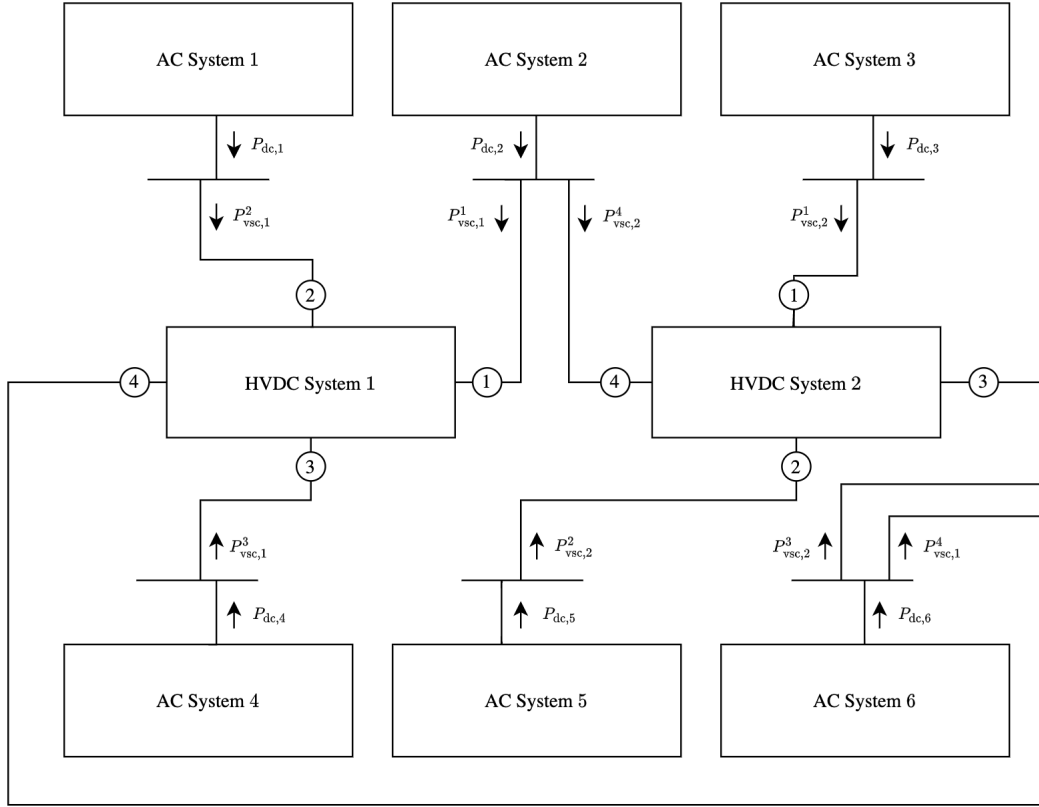


Figure 5.1: Topology of the Overall Test System

It is assumed that the operating point of the MTDC system is determined by scheduled power transfer between the AC and DC systems as summarized in Table 5.1.

$h$	$\bar{P}_{dc,h}$ (MW)
1	604.00
2	-993.98
3	-557.47
4	402.27
5	441.23
6	-75.58

Table 5.1: Scheduled power transfer between AC systems

The nominal voltage of the HVDC system is 400 kV; that is  $V_{dc,l}^{\text{nom}} = 400 \times 10^3$ . Tables 5.2 and 5.3 summarize the operating point bus voltages and line currents of the HVDC test systems corresponding to the scheduled power transfer between AC systems.

Bus $k$	$\bar{V}_{dc,1}^k$ (kV)	$\bar{V}_{dc,2}^k$ (kV)
1	397.28	398.19
2	402.67	401.12
3	402.27	402.79
4	398.37	398.92
5	397.98	398.66
6	402.47	401.91
7	398.95	399.39

Table 5.2: Operating point bus voltage in HVDC test systems

Line $k$	$\bar{I}_{L,1}^k$ (kA)	$\bar{I}_{L,2}^k$ (kA)
1	1.30	1.40
2	-0.10	0.20
3	-1.40	-1.30
4	-1.00	-1.20
5	1.40	1.20
6	0.40	-0.10

Table 5.3: Operating point link currents of HVDC test systems

Table 5.4 summarizes the operating point power injected  $\bar{P}_{inj,l}^k$  into the HVDC test systems at each bus. It should be noted that  $\bar{P}_{inj,l}^k = \bar{P}_{vsc,l}^k$  for  $k = 1, \dots, 4$ . The power injected at the remaining buses  $\bar{P}_{inj,l}^k$  for  $k \in \{5, 6, 7\}$  represent the DC power supplied or demanded by DC sources or loads respectively.

Bus $k$	$\bar{P}_{inj,1}^k$ (MW)	$\bar{P}_{inj,2}^k$ (MW)
1	-516.5	-557.5
2	604.0	441.2
3	402.3	482.1
4	-557.7	-477.5
5	-159.2	40.0
6	1,046.4	1,125.4
7	-797.9	-1,038.4

Table 5.4: Operating point power injected into the HVDC test systems at each bus

### 5.1.1 HVDC Test Systems Parameters

We consider two ( $M = 2$ ) HVDC test systems comprising of seven buses,  $n_{dc,1} = n_{dc,2} = 7$ , and six lines,  $m_{dc,1} = m_{dc,2} = 6$ , as depicted in Figure 5.2. Each HVDC system has four VSC buses connecting AC and DC terminals, i.e.,  $p_1 = p_2 = 4$ .

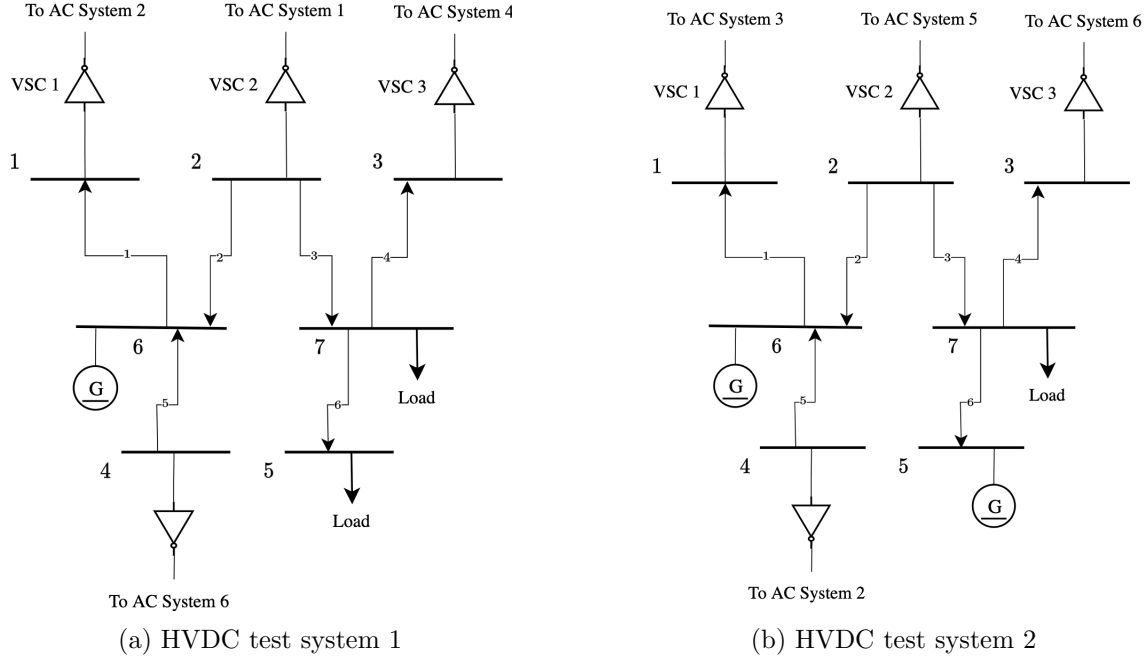


Figure 5.2: Topology of HVDC test systems

Each converter DC-side capacitor is 120  $\mu\text{F}$ , i.e.,  $C_{\text{dc},1}^i = C_{\text{dc},2}^i = 120 \mu\text{F}$  for  $i \in \{1, 2, 3, 4\}$  and  $C_{\text{dc},1}^i = C_{\text{dc},2}^i = 0 \text{ F}$  for  $i \in \{5, 6, 7\}$  [39]. The  $\Pi$ -link parameters and lengths for DC lines in both systems are summarized in the below tables [40].

Line Parameter	$R$ ( $\Omega/\text{km}$ )	$L$ (mH/km)	$C_{\Pi}$ ( $\mu\text{F}/\text{km}$ )
Value	0.0133	0.8273	0.0139

Table 5.5: Grid line parameters of HVDC test systems

Line Number	System 1 (km)	System 2 (km)
1	300	200
2	150	300
3	200	100
4	250	150
5	220	250
6	180	200

Table 5.6: Grid line lengths of HVDC test systems

### 5.1.2 AC Test Systems Parameters

For the AC test systems, the below table summarizes the parameters of the aggregated generator representing each of the AC test systems:

Parameter	System 1	System 2	System 3	System 4	System 5	System 6	Unit
$J_h$	23,120	22,300	21,520	22,340	24,230	23,720	kg.m <sup>2</sup>
$D_{g,h}$	446.45	445.78	450.7	449.9	448.43	445.97	W.s <sup>2</sup>
$T_{m,h}$	1.5	2.0	2.5	2.0	1.5	2.5	s
$\sigma_h$	0.02	0.02	0.02	0.02	0.02	0.02	/
$D_{l,h}$	0.1	0.05	0.06	0.1	0.1	0.08	s
$P_{\text{nom},h}$	2,000	2,000	2,000	2,000	2,000	2,000	MW

Table 5.7: Parameters of AC test systems

Parameter	System 1	System 2	System 3	System 4	System 5	System 6	Unit
$f_{\text{nom},h}$	50	50	50	50	50	50	Hz
$\bar{P}_{m,h}^0$	2,000	2,000	2,000	2,000	2,000	2,000	MW
$\bar{P}_{l,h}^0$	1,396	2,994	2,557	1,598	1,559	2,076	MW

Table 5.8: Operating point values of AC test systems

The AC system parameters summarized in Tables 5.7 and 5.8 do not represent real physical systems/models. Parameters are chosen such that they give logical and physically accepted frequency and mechanical power wave-forms upon simulation. The parameter values are taken from [37] and adjusted to increase the size of the AC systems while maintaining comparable  $D_h/J_h$  ratios to that of the test systems in [37]. This will result in obtaining similar transient and steady-state characteristics of the system variables in response to power load disturbance as verified in the dashed wave-forms in Figures 5.3 and 5.9.

## 5.2 Cost Function Parameters

Consider the cost function (4.18). We define  $M_f$  such that the marginal cost of frequency deviation per unit Hz of systems 2, 3, and 6 is 1.5 times higher than that of systems 1 and 5, and that of 4 is twice that of system 1 such that  $M_f = \text{diag}(1, 1.5, 1.5, 2, 1, 1.5)^1$ . We tune  $\tau$  such that the LC-OSS controller responds to power load variations faster than the governors with  $\tau = 5 \text{ s/MW}^2$ .

We consider three different tunings of the same controller (4.22) to illustrate the options and flexibility inherent in the OSS control framework by adjusting the values of  $\alpha_p$ ,  $\alpha_f$ , and  $\alpha_i$ . The tuple  $(\alpha_{p,i}, \alpha_{f,i}, \alpha_{i,i})$  defines the cost function  $f_i(y)$  for  $i \in \{1, 2, 3\}$ . Table 5.9 summarizes the different tunings of  $(\alpha_{p,i}, \alpha_{f,i}, \alpha_{i,i})$ .

<sup>1</sup>The elements of  $M_f$  are unit-less as the unit is incorporated in  $\alpha_f$  as stated in Table 5.9

$i$	$\alpha_{p,i}$ (1/W <sup>2</sup> )	$\alpha_{f,i}$ (1/Hz <sup>2</sup> )	$\alpha_{i,i}$ (1/A <sup>2</sup> )
1	$10^{-2}$	$2 \times 10^7$	0
2	$5 \times 10^{-2}$	$10^7$	0
3	$5 \times 10^{-2}$	$10^7$	15

Table 5.9: Parameters of cost functions  $f_1(y)$ ,  $f_2(y)$ , and  $f_3(y)$ 

The cost functions associated to the three tunings are defined as follows:

1. The first cost function  $f_1(y)$  sets high penalty cost on frequency deviation of AC systems. The OSS controller associated to  $f_1(y)$  is expected to result in the least frequency deviation among the three controllers.
2. The second cost function  $f_2(y)$  sets high penalty on power loss in HVDC systems. The OSS controller associated to  $f_2(y)$  is expected to compromise frequency deviation with reduced power loss in HVDC systems.
3. The third cost function  $f_3(y)$  sets high penalty on power loss in HVDC systems while enforcing the soft inequality constraint on current limits. The OSS controller associated to  $f_3(y)$  is expected to behave similar to that associated to  $f_2(y)$  with some of the DC link currents hitting saturation.

**Remark 5.2.1.** Although the current limit capacity of the chosen DC lines is  $\pm 3$  kA [40], we will artificially lower the current limit capacity of the DC lines to  $\pm 1.5$  kA to activate the controller associated to  $f_3(y)$  such that  $I_{L,l}^{\min} = I_L^{\min} = -1.5$  kA and  $I_{L,l}^{\max} = I_L^{\max} = 1.5$  kA for  $l \in \{1, 2\}$ .

### 5.3 Results

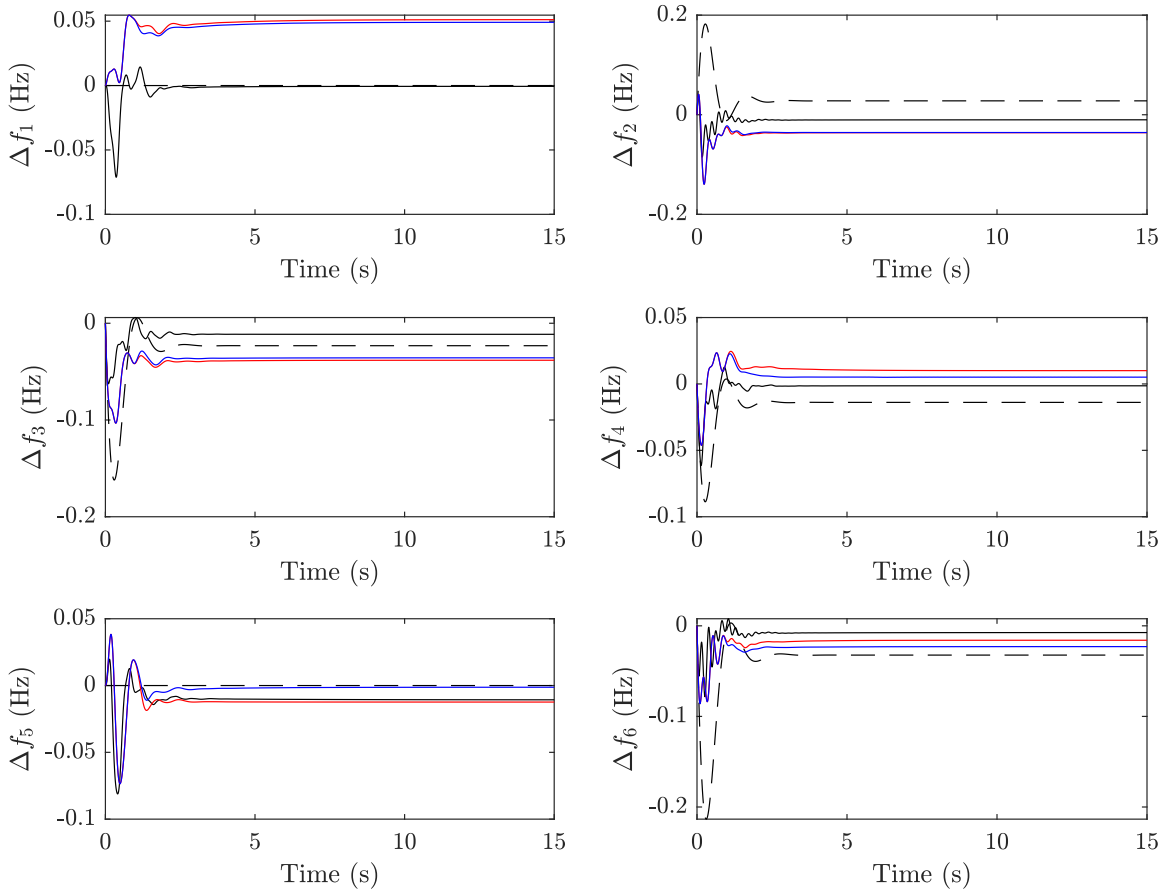
It is assumed that the systems are operating at their respective operating point as in Tables 5.3 and 5.8. Table 5.10 summarizes the power load disturbance  $\Delta P_{1,h}(t)$  for  $h \in \{2, 3, 4, 6\}$  imposed on AC systems 2, 3, 4, and 6.

Load change in AC System $h$	$w_{ac,h} = \Delta P_{1,h}^0$ (MW)
2.0% decrease in $P_{1,2}^0$	-60
2.0% increase in $P_{1,3}^0$	50
1.9% increase in $P_{1,4}^0$	30
3.4% increase in $P_{1,6}^0$	70

Table 5.10: AC systems' load power disturbance

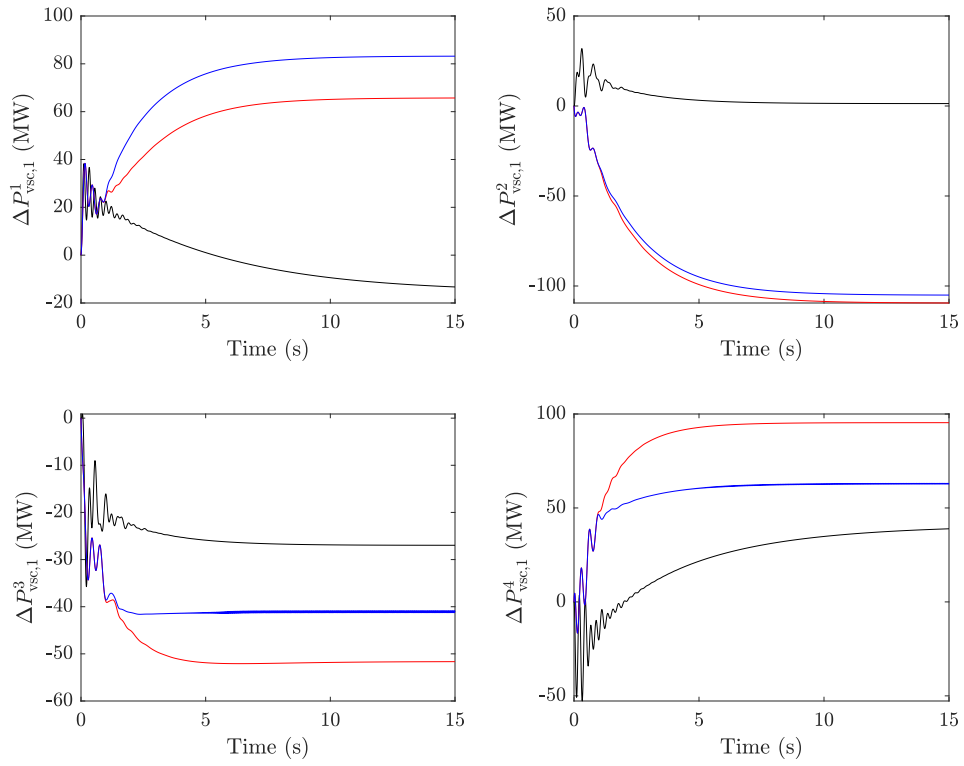
Figure 5.3 shows the frequency deviation of the AC systems with and without implementing the controllers. The overall frequency deviation in the disturbed AC

systems has been reduced with all three controllers. This is due to the distribution of the burden of power load imbalance over all AC systems. Systems 1 and 5, which are originally undisturbed, now witness disturbance transferred from the remaining systems through the HVDC systems. The frequency deviation is most reduced with controller 1 as it allocates double the weight on frequency deviation as compared to that of controllers 2 and 3. In addition, controllers 2 and 3 allocate higher weight on power loss in HVDC systems which further reduces the capability of the controller to minimize frequency deviation.

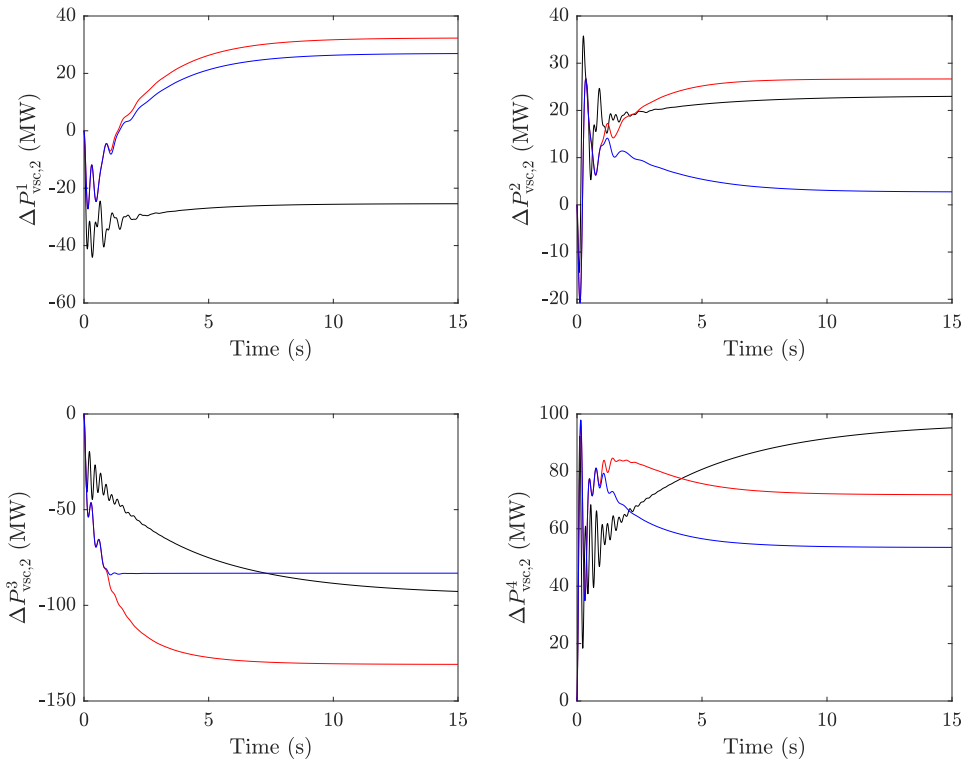
Figure 5.3:  $\Delta f$  of AC Systems

--- No controller — OSS with  $f_1(y)$  — OSS with  $f_2(y)$  — OSS with  $f_3(y)$

The power transferred by each of the VSC's in HVDC systems 1 and 2 is shown in Figure 5.5. It can be evidently seen that the OSS controller dispatches power transfer commands to the VSCs before the governors of the AC systems take action (See Figure 5.9). Hence, governors now respond to a power load variation that has been adjusted by the faster OSS control.



(a) HVDC system 1



(b) HVDC system 2

Figure 5.5:  $\Delta P_{\text{vsc}}$  of the HVDC systems

— OSS with  $f_1(y)$  — OSS with  $f_2(y)$  — OSS with  $f_3(y)$

Figure 5.7 demonstrates the adjusted power load imbalance  $\hat{w}_{ac} := w_{ac} + \Delta P_{dc}$  that the governor of each of the AC systems should mitigate. The power load imbalance of systems 2, 3, 4, and 6 is reduced transferring some of the power load imbalance to the undisturbed systems 1 and 5.

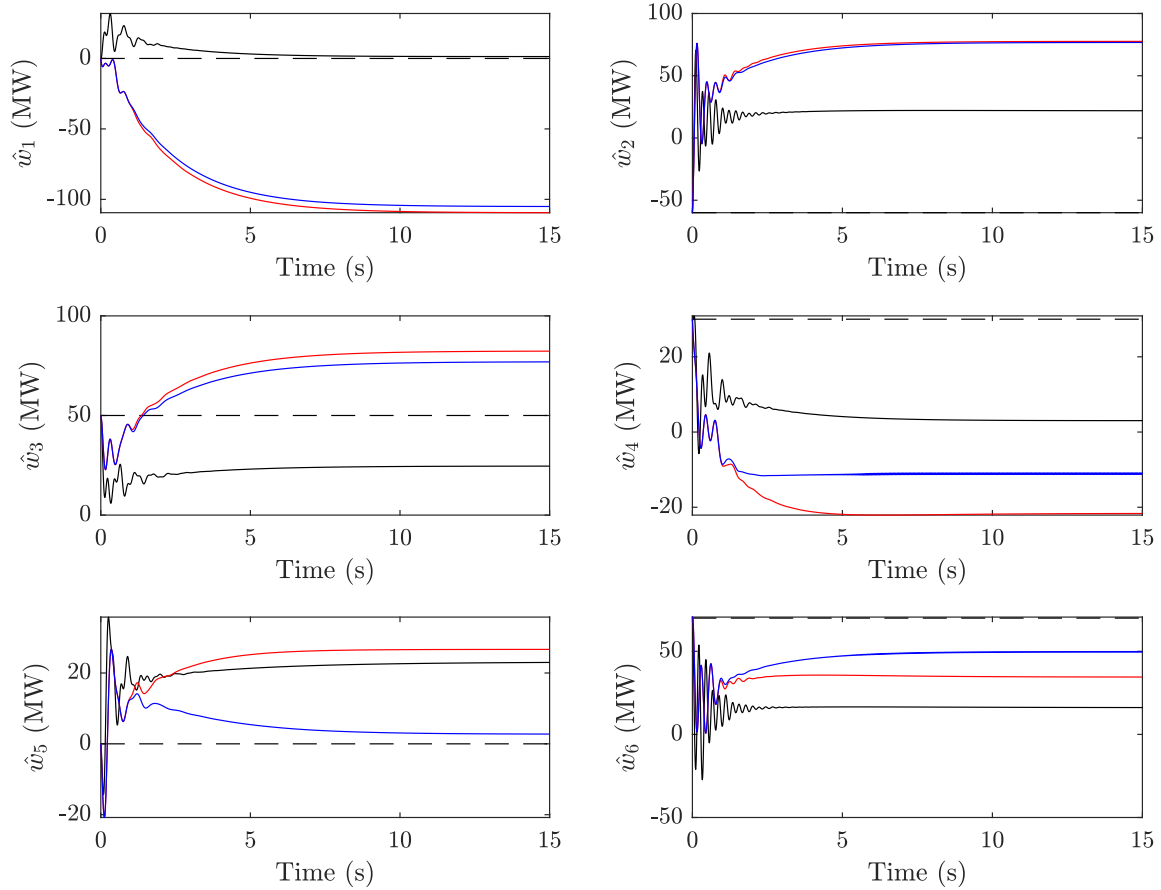


Figure 5.7: Adjusted power load disturbance in AC systems

----- No controller    ——— OSS with  $f_1(y)$     ——— OSS with  $f_2(y)$     ——— OSS with  $f_3(y)$

All three controllers are achieving distribution of primary frequency reserves between AC systems as the burden of power load imbalance in systems 2, 3, 4, and 6 is now shared between all systems including the undisturbed systems 1 and 5. As a result, less reserve power is required to be supplied by the governors, and this can be evidently seen in Figure 5.9.

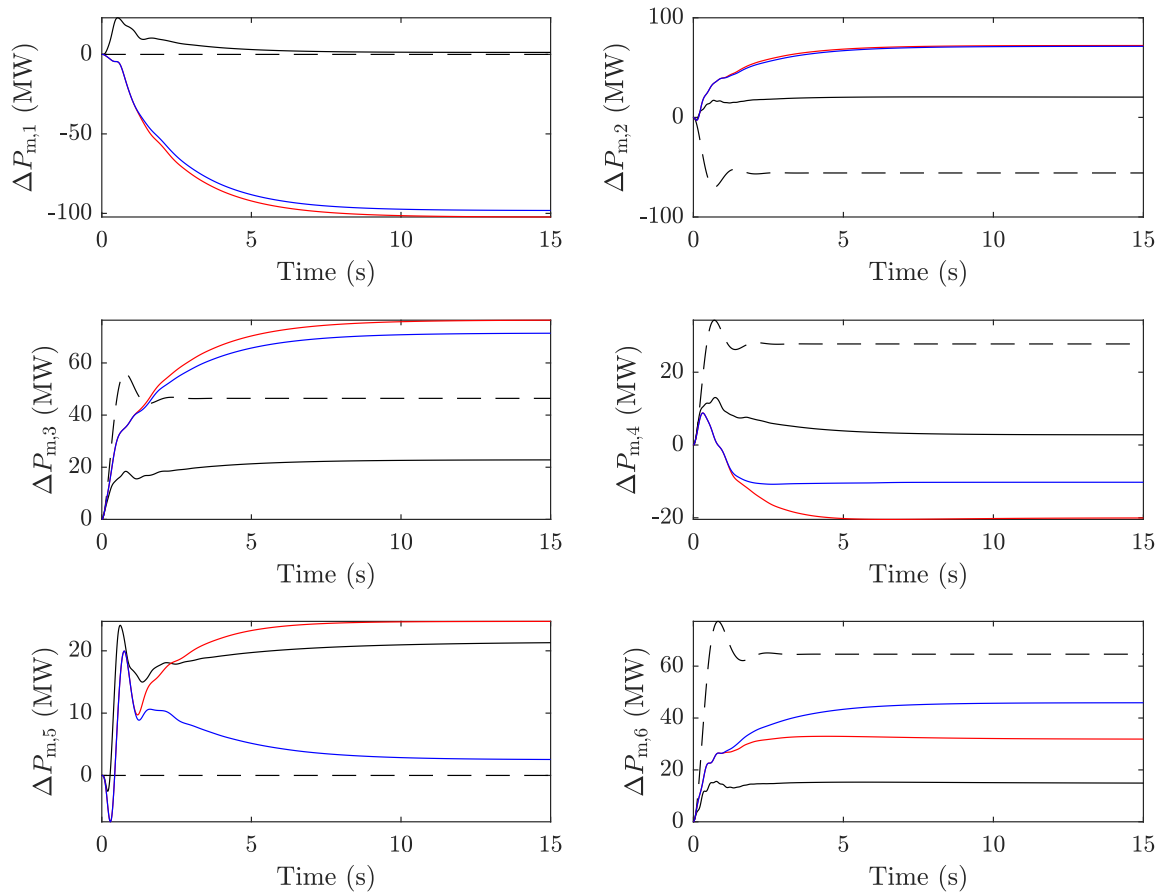
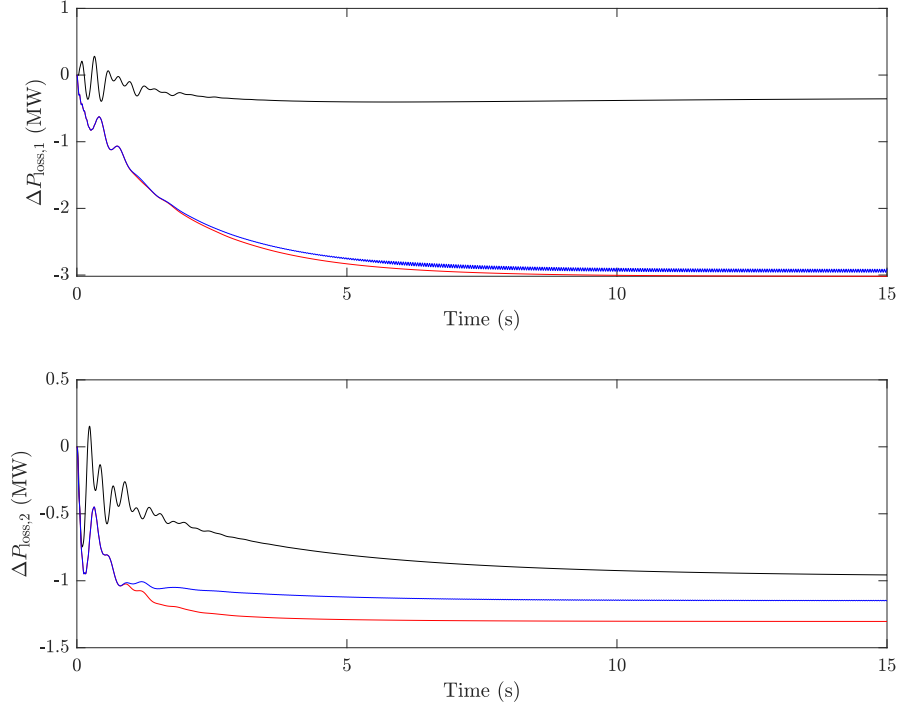


Figure 5.9:  $\Delta P_m$  of AC Systems

----- No controller    ——— OSS with  $f_1(y)$     ——— OSS with  $f_2(y)$     ——— OSS with  $f_3(y)$

Since  $\alpha_p$  is 5 times greater in controllers 2 and 3 than in controller 1, reduction in power loss in HVDC systems with controllers 2 and 3 is greater than that with controller 1 as seen in Figure 5.11.

Figure 5.11:  $\Delta P_{\text{loss}}$  of HVDC systems 1 and 2

— OSS with  $f_1(y)$  — OSS with  $f_2(y)$  — OSS with  $f_3(y)$

Finally, since we enforce stricter inequality constraints on the current limits with a greater  $\alpha_i$  in controller 3, we notice current saturation in some of the HVDC lines. In HVDC system 1, current in line 3 saturates at  $-100$  A, i.e.,  $i_{L,1}^3$  saturates at  $I_L^{\min} - \bar{I}_{L,1}^3 = -1.5 - (-1.4) = -0.1$  kA. In HVDC system 2, current in line 3 saturates at  $-200$  A, i.e.,  $i_{L,2}^3$  saturates at  $I_L^{\min} - \bar{I}_{L,2}^3 = -1.5 - (-1.3) = -0.2$  kA.

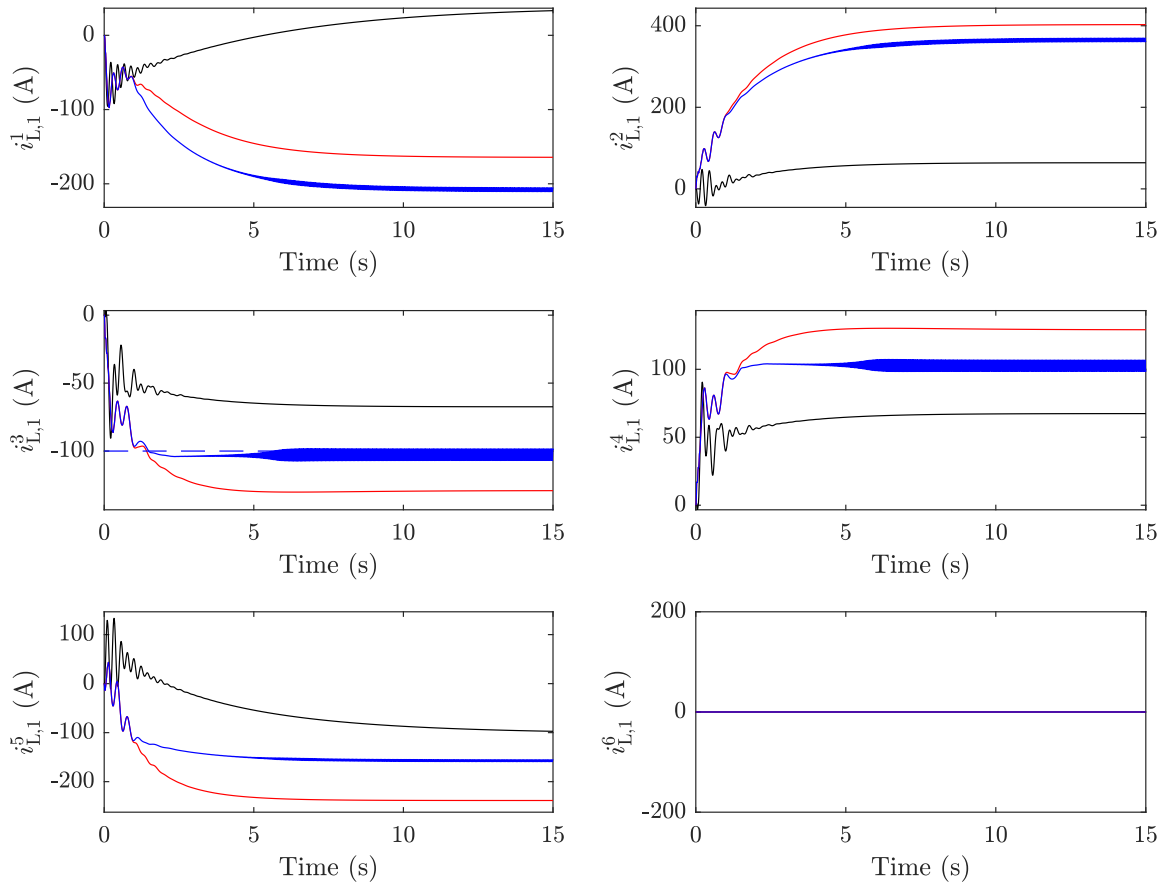


Figure 5.13:  $i_{L,1}$  of HVDC system 1

— OSS with  $f_1(y)$  — OSS with  $f_2(y)$  — OSS with  $f_3(y)$  - - - Current limit

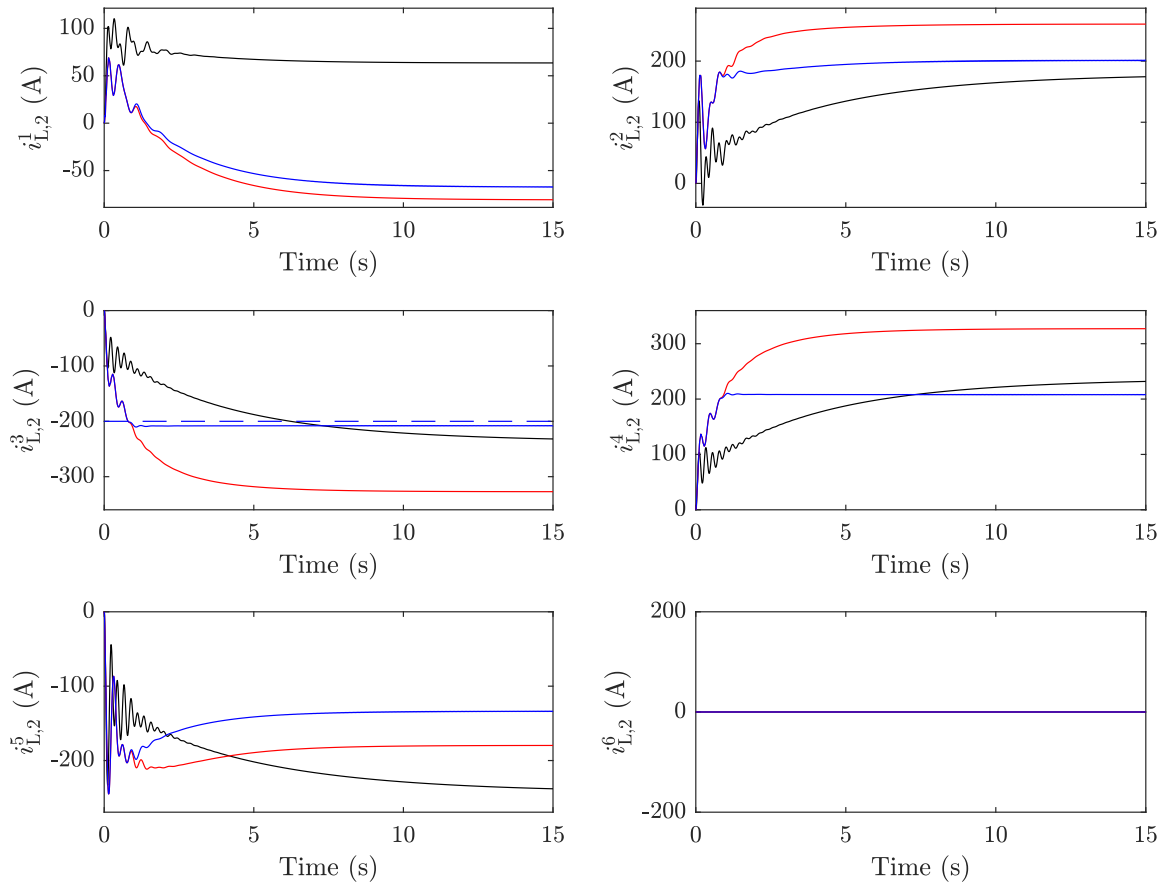


Figure 5.15:  $i_{L,2}$  of HVDC system 2

— OSS with  $f_1(y)$  — OSS with  $f_2(y)$  — OSS with  $f_3(y)$  - - - Current limit

## Chapter 6

# Conclusion and Future Work

### 6.1 Conclusion

In this thesis we adopt the linear-convex optimal steady state control framework to control multi terminal high-voltage DC systems.

There are three major components in this thesis. We first prove that the LC-OSS control encompasses some of the existing MTDC controllers in the literature. We recover two different MTDC controllers; a distributed power consensus controller and a decentralized voltage controller. For each of the controllers recovered, we provide a stability analysis of the closed-loop system.

In the second component, we adopt the LC-OSS framework to develop an output feedback controller for an MTDC system. We propose a dynamic controller which drives the AC systems to collectively respond to power load variation happening in some of them while minimizing DC losses and maintaining DC line currents within acceptable limits. We also provide a stability analysis of the system closed by a simplified version of the controller.

In the last component, we apply the proposed controller to an MTDC test system. The controller's performance is evaluated based on a time-domain simulation in MATLAB/Simulink environment. We verify that the controller is able to drive the MTDC test system to the optimal operating point which meets the control objectives.

### 6.2 Future Work

Immediate future research directions complementing the work of this thesis are as follows:

- **Stability Analysis:** Although the numerical results verify that the proposed feedback controller stabilizes the closed-loop system for the convex cost func-

tion (4.18), the stability analysis conducted in Chapter 4 drops the inequality enforcing and power loss cost functions. A future research direction is to prove the stability of the closed system including all components of (4.18). This will require nonlinear control theory tools. Another future research direction is to prove stability of the system by dropping Assumption 4.4.1; that is for the cases whereby  $\text{rank}(\mathcal{C}^\top S) < N$ .

- **Modeling and Control:** In this thesis, we adopt a linearized state-space model of the HVDC system by Assumption 3.2.2. A future research area to be investigated is releasing this assumption and applying the general nonlinear OSS framework [41]. Furthermore, the current controller set-up assumes no saturation limits on the power transferred via VSCs which could potentially lead to physically unacceptable control commands dispatched by the OSS controller to the VSCs. A future research direction is applying constraints on VSCs.
- **Testing:** The numerical analysis performed in this thesis is based on the time-domain simulation of an LTI state-space model on MATLAB/Simulink. Further testing can be applied on more sophisticated simulation platforms such as PSCAD to fully capture all system dynamics. The testing can also be applied on standard AC test systems.

# Appendix A

## Chapter 3 Supplements

### A.1 Linearization of the AC System Model

Consider the non-linear differential equation governing the electro-mechanical dynamics of AC system  $h$  in (3.6a) and (3.6c) which is given by

$$J_h \dot{f}_h = \frac{P_{m,h} - P_{1,h}^0 (1 + D_{1,h}(f_h - f_{\text{nom},h})) - P_{\text{dc},h}}{4\pi^2 f_h} - D_{g,h}(f_h - f_{\text{nom},h}). \quad (\text{A.1})$$

Let  $x_{\text{gen}}$  represent the state vector and  $u_{\text{gen}}$  the input vector of (A.1) such that

$$\begin{aligned} x_{\text{gen}} &:= \text{col}(f_h, P_{m,h}), \\ u_{\text{gen}} &:= \text{col}(P_{\text{dc},h}, P_{m,h}^0, P_{1,h}^0). \end{aligned}$$

We denote the right-hand-side of (A.1) by  $h(x_{\text{gen}}, u_{\text{gen}})$  such that

$$h(x_{\text{gen}}, u_{\text{gen}}) := \frac{P_{m,h} - P_{1,h}^0 (1 + D_{1,h}(f_h - f_{\text{nom},h})) - P_{\text{dc},h}}{4\pi^2 f_h} - D_{g,h}(f_h - f_{\text{nom},h}).$$

Let  $(\bar{x}_{\text{gen}}, \bar{u}_{\text{gen}})$  represent an equilibrium operating point of the system (3.6) such that

$$\begin{aligned} \bar{x}_{\text{gen}} &:= \text{col}(\bar{f}_h, \bar{P}_{m,h}), \\ \bar{u}_{\text{gen}} &:= \text{col}(\bar{P}_{\text{dc},h}, \bar{P}_{m,h}^0, \bar{P}_{1,h}^0), \end{aligned}$$

whereby the components of  $(\bar{x}_{\text{gen}}, \bar{u}_{\text{gen}})$  are derived in Section 3.3.

A linearized equivalent of (A.1) around the defined operating point can be obtained

by:

$$\begin{aligned}
J_h \Delta \dot{f}_h &= \underbrace{\frac{\partial h(\bar{x}_{\text{gen}}, \bar{u}_{\text{gen}})}{\partial f_h} \Delta f_h}_{(1)} + \underbrace{\frac{\partial h(\bar{x}_{\text{gen}}, \bar{u}_{\text{gen}})}{\partial P_{m,h}} \Delta P_{m,h}}_{(2)} \\
&+ \underbrace{\frac{\partial h(\bar{x}_{\text{gen}}, \bar{u}_{\text{gen}})}{\partial P_{\text{dc},h}} \Delta P_{\text{dc},h}}_{(3)} + \underbrace{\frac{\partial h(\bar{x}_{\text{gen}}, \bar{u}_{\text{gen}})}{\partial P_{m,h}^0} \Delta P_{m,h}^0}_{(4)} + \underbrace{\frac{\partial h(\bar{x}_{\text{gen}}, \bar{u}_{\text{gen}})}{\partial P_{1,h}^0} \Delta P_{1,h}^0}_{(5)},
\end{aligned}$$

where deviation state variables  $(\Delta f_h, \Delta P_{m,h})$ , and deviation input variables  $(\Delta P_{\text{dc},h}, \Delta P_{m,h}^0, \Delta P_{1,h}^0)$  are defined in Section 3.3.

Deriving the expressions of (1)-(5), we get

$$\begin{aligned}
(1) &= \frac{\overbrace{\bar{P}_{m,h} - \bar{P}_{1,h}^0 - \bar{P}_{\text{dc},h}}{=0}}{4\pi^2 \bar{f}_h^2} \Delta f_h + \left( -D_{g,h} - \frac{\bar{P}_{1,h}^0 D_{1,h}}{4\pi^2 \bar{f}_h} \right) \Delta f_h = - \left( D_{g,h} + \frac{\bar{P}_{1,h}^0 D_{1,h}}{4\pi^2 f_{\text{nom},h}} \right) \Delta f_h, \\
(2) &= \frac{\Delta P_{m,h}}{4\pi^2 \bar{f}_h} = \frac{\Delta P_{m,h}}{4\pi^2 f_{\text{nom},h}}, \\
(3) &= \frac{-\Delta P_{\text{dc},h}}{4\pi^2 \bar{f}_h} = \frac{-\Delta P_{\text{dc},h}}{4\pi^2 f_{\text{nom},h}}, \\
(4) &= \frac{\partial h(\bar{x}_{\text{gen}}, \bar{u}_{\text{gen}})}{\partial P_{1,h}^0} \underbrace{\Delta P_{m,h}^0}_{=0} = 0, \\
(5) &= \frac{-(1 + D_{1,h}(\bar{f}_h - f_{\text{nom},h}))}{4\pi^2 \bar{f}_h} \Delta P_{1,h}^0 = \frac{-(1 + D_{1,h}(f_{\text{nom},h} - f_{\text{nom},h}))}{4\pi^2 f_{\text{nom},h}} \Delta P_{1,h}^0 = \frac{-\Delta P_{1,h}^0}{4\pi^2 f_{\text{nom},h}}.
\end{aligned}$$

Substituting, we get a linearized version of the swing equation of (A.1) such that

$$J_h \Delta \dot{f}_h = \frac{\Delta P_{m,h} - \Delta P_{1,h}^0 - \Delta P_{\text{dc},h}}{4\pi^2 f_{\text{nom},h}} - \left( D_{g,h} + \frac{\bar{P}_{1,h}^0 D_{1,h}}{4\pi^2 f_{\text{nom},h}} \right) \Delta f_h.$$

# Appendix B

## Chapter 4 Supplements

### B.1 Derivation of the expression of $\tilde{G}_\eta(0)$

From section 4.1.1,  $\tilde{G}_\eta(0) = -\tilde{C}\tilde{A}^{-1}B$  is defined to be the DC gain matrix of system  $\beta$ , which is the system (4.7) closed by the proportional controller  $u = \beta\tilde{y}$  as depicted in figure B.1.

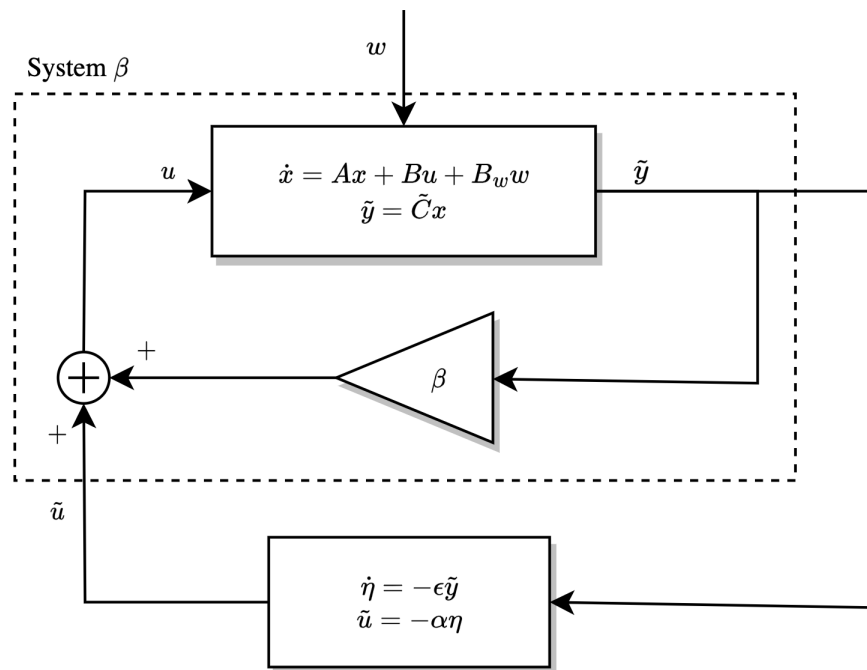


Figure B.1: Block diagram of the system (4.7)-(4.8)

Ignoring the disturbance  $w$ , the state-space model of system  $\beta$  is given by

$$\begin{bmatrix} \Delta \dot{f} \\ \Delta \dot{P}_m \end{bmatrix} = \underbrace{\begin{bmatrix} -J^{-1}\mathcal{D} - \beta J^{-1}\mathcal{L}_c & J^{-1} \\ -T_m^{-1}K & -T_m^{-1} \end{bmatrix}}_{\bar{A}=A+\beta B\bar{C}} \begin{bmatrix} \Delta f \\ \Delta P_m \end{bmatrix} + \begin{bmatrix} -J^{-1} \\ \mathbb{0} \end{bmatrix} \tilde{u}.$$

At steady state,  $\Delta \dot{f} = 0$  and  $\Delta \dot{P}_m = 0$  which results in

$$\begin{aligned} \Delta \bar{P}_m &= -K \Delta f, \\ \Delta \bar{f} &= -(\mathcal{D} + K + \beta \mathcal{L}_c)^{-1} \tilde{u}. \end{aligned}$$

Therefore, the steady state mapping that maps  $\tilde{u}$  to  $\tilde{y}$  is given by

$$\tilde{y} = \mathcal{L}_c \Delta \bar{f} = \underbrace{-\mathcal{L}_c (\mathcal{D} + K + \beta \mathcal{L}_c)^{-1}}_{\tilde{G}_\eta(0)} \tilde{u}.$$

## B.2 System Steady State Derivation

In this section, we derive the expressions of the steady state DC voltages and link currents corresponding to HVDC system  $l$ . Consider the equilibrium equation

$$\begin{bmatrix} \mathbb{0} & -C_l^{-1} F_{dc,l} \\ L_l^{-1} F_{dc,l}^\top & -L_l^{-1} R_l \end{bmatrix} \begin{bmatrix} \bar{v}_{dc,l} \\ \bar{i}_{L,l} \end{bmatrix} + \begin{bmatrix} \frac{1}{V_{dc,l}^{nom}} C_{pi}^{-1} \\ \mathbb{0} \end{bmatrix} \bar{u}_l = \mathbb{0}. \quad (\text{B.1})$$

We left multiply the first  $n_{dc,l}$  rows by  $C_l$  and the last  $m_{dc,l}$  rows by  $L_l$  to obtain

$$-F_{dc,l} \bar{i}_{L,l} + \begin{bmatrix} \frac{1}{V_{dc,l}^{nom}} \bar{u}_l \\ \mathbb{0} \end{bmatrix} = \mathbb{0} \quad (\text{B.2})$$

$$F_{dc,l}^\top \bar{v}_{dc,l} - R_l \bar{i}_{L,l} = \mathbb{0}. \quad (\text{B.3})$$

Left multiply (B.2) by  $\mathbb{1}^\top$ , we deduce that  $\mathbb{1}^\top \bar{u}_l = 0$ . This applies for all the  $M$  HVDC networks, hence  $\mathbb{1}^\top \bar{u}_1 = \dots = \mathbb{1}^\top \bar{u}_M = 0$ , which implies that  $\mathbb{1}^\top \bar{u} = 0$ .

From (B.3),  $\bar{i}_{L,l}$  can be written as

$$\bar{i}_{L,l} = R_l^{-1} F_{dc,l}^\top \bar{v}_{dc,l}.$$

Substituting back in (B.2), we get

$$-\mathcal{L}_{\text{dc},l}\bar{v}_{\text{dc},l} + \begin{bmatrix} \frac{1}{V_{\text{dc},l}^{\text{nom}}}\bar{u}_l \\ \mathbf{0} \end{bmatrix} = \mathbf{0},$$

where  $\mathcal{L}_{\text{dc},l}$  for  $l = 1, \dots, M$  is the weighted Laplacian matrix of the graph describing HVDC grid  $l$  which is defined as  $\mathcal{L}_{\text{dc},l} := F_{\text{dc},l}R_l^{-1}F_{\text{dc},l}^\top$ .

Therefore,  $\bar{v}_{\text{dc},l}$  and  $\bar{i}_{L,l}$  are given by:

$$\begin{aligned} \bar{v}_{\text{dc},l} &= \frac{1}{V_{\text{dc},l}^{\text{nom}}}\mathcal{L}_{\text{dc},l}^\dagger \begin{bmatrix} I_{p_l} \\ \mathbf{0} \end{bmatrix} \bar{u}_l + \beta_l \mathbf{1}, \\ \bar{i}_{L,l} &= R_l^{-1}F_{\text{dc},l}^\top \left( \frac{1}{V_{\text{dc},l}^{\text{nom}}}\mathcal{L}_{\text{dc},l}^\dagger \begin{bmatrix} I_{p_l} \\ \mathbf{0} \end{bmatrix} \bar{u}_l + \beta_l \mathbf{1} \right). \end{aligned}$$

where, for  $l = 1, \dots, M$ ,  $\beta_l \in \mathbb{R}$  is a free variable.

# Bibliography

- [1] *Milestones: Gotland high voltage direct current link, 1954*. [Online]. Available: [https://ethw.org/Milestones:Gotland\\_High\\_Voltage\\_Direct\\_Current\\_Link,\\_1954#Title](https://ethw.org/Milestones:Gotland_High_Voltage_Direct_Current_Link,_1954#Title).
- [2] R. Adapa, “High-wire act: HvdC technology: The state of the art,” *IEEE Power and Energy Magazine*, vol. 10, no. 6, pp. 18–29, 2012. DOI: 10.1109/MPE.2012.2213011.
- [3] D. Van Hertem, O. Gomis-Bellmunt, and J. Liang, *HVDC grids: for offshore and supergrid of the future*. John Wiley & Sons, 2016.
- [4] D. Jovcic, *High voltage direct current transmission: converters, systems and DC grids*. John Wiley & Sons, 2019.
- [5] W. F. Long, J. Reeve, J. R. McNichol, *et al.*, “Application aspects of multiterminal dc power transmission,” 1990.
- [6] A. Yazdani and R. Iravani, *Voltage-sourced converters in power systems: modeling, control, and applications*. John Wiley & Sons, 2010.
- [7] J. Arrillaga, N. R. Watson, and Y. Liu, *Flexible power transmission: the HVDC options*. John Wiley & Sons, 2007.
- [8] D. Van Hertem and M. Ghandhari, “Multi-terminal vsc hvdc for the european supergrid: Obstacles,” *Renewable and sustainable energy reviews*, vol. 14, no. 9, pp. 3156–3163, 2010.
- [9] N. Chaudhuri, B. Chaudhuri, R. Majumder, and A. Yazdani, *Multi-terminal direct-current grids: Modeling, analysis, and control*. John Wiley & Sons, 2014.
- [10] T. K. Vrana, J. Beerten, R. Belmans, and O. B. Fosso, “A classification of dc node voltage control methods for hvdc grids,” *Electric Power Systems Research*, vol. 103, pp. 137–144, 2013, ISSN: 0378-7796. DOI: <https://doi.org/10.1016/j.epsr.2013.05.001>. [Online]. Available: <https://www.sciencedirect.com/science/article/pii/S0378779613001193>.
- [11] R. T. Pinto, S. F. Rodrigues, P. Bauer, and J. Pierik, “Comparison of direct voltage control methods of multi-terminal dc (mtdc) networks through modular dynamic models,” in *Proceedings of the 2011 14th European Conference on Power Electronics and Applications*, 2011, pp. 1–10.

- [12] T. Nakajima and S. Irokawa, "A control system for hvdc transmission by voltage sourced converters," in *1999 IEEE Power Engineering Society Summer Meeting. Conference Proceedings (Cat. No.99CH36364)*, vol. 2, 1999, 1113–1119 vol.2. DOI: 10.1109/PESS.1999.787474.
- [13] R. Teixeira Pinto, P. Bauer, S. F. Rodrigues, E. J. Wiggelinkhuizen, J. Pierik, and B. Ferreira, "A novel distributed direct-voltage control strategy for grid integration of offshore wind energy systems through mtde network," *IEEE Transactions on Industrial Electronics*, vol. 60, no. 6, pp. 2429–2441, 2013. DOI: 10.1109/TIE.2012.2216239.
- [14] J. Dai, Y. Phulpin, A. Sarlette, and D. Ernst, "Coordinated primary frequency control among non-synchronous systems connected by a multi-terminal high-voltage direct current grid," *IET generation, transmission & distribution*, vol. 6, no. 2, pp. 99–108, 2012.
- [15] —, "Voltage control in an hvdc system to share primary frequency reserves between non-synchronous areas," 2011.
- [16] B. Silva, C. Moreira, L. Seca, Y. Phulpin, and J. P. Lopes, "Provision of inertial and primary frequency control services using offshore multiterminal hvdc networks," *IEEE Transactions on Sustainable Energy*, vol. 3, no. 4, pp. 800–808, 2012.
- [17] M. Andreasson, R. Wiget, D. V. Dimarogonas, K. H. Johansson, and G. Andersson, "Distributed primary frequency control through multi-terminal hvdc transmission systems," in *2015 American Control Conference (ACC)*, IEEE, 2015, pp. 5029–5034.
- [18] J. Dai and G. Damm, "An improved control law using hvdc systems for frequency control," in *Power systems computation conference*, 2011.
- [19] A. Sarlette, J. Dai, Y. Phulpin, and D. Ernst, "Cooperative frequency control with a multi-terminal high-voltage dc network," *Automatica*, vol. 48, no. 12, pp. 3128–3134, 2012.
- [20] A. Kiani Bejestani, A. Annaswamy, and T. Samad, "A hierarchical transactive control architecture for renewables integration in smart grids: Analytical modeling and stability," *IEEE Transactions on Smart Grid*, vol. 5, no. 4, pp. 2054–2065, 2014. DOI: 10.1109/TSG.2014.2325575.
- [21] Y. Tang, K. Dvijotham, and S. Low, "Real-time optimal power flow," *IEEE Transactions on Smart Grid*, vol. 8, no. 6, pp. 2963–2973, 2017. DOI: 10.1109/TSG.2017.2704922.
- [22] A. Jokic, M. Lazar, and P. P. J. van den Bosch, "On constrained steady-state regulation: Dynamic kkt controllers," *IEEE Transactions on Automatic Control*, vol. 54, no. 9, pp. 2250–2254, 2009. DOI: 10.1109/TAC.2009.2026856.
- [23] M. Colombino, E. Dall’Anese, and A. Bernstein, "Online optimization as a feedback controller: Stability and tracking," *IEEE Transactions on Control of Network Systems*, vol. 7, no. 1, pp. 422–432, 2020. DOI: 10.1109/TCNS.2019.2906916.

- [24] M. Colombino, J. W. Simpson-Porco, and A. Bernstein, “Towards robustness guarantees for feedback-based optimization,” in *2019 IEEE 58th Conference on Decision and Control (CDC)*, 2019, pp. 6207–6214. DOI: 10.1109/CDC40024.2019.9029953.
- [25] S. Menta, A. Hauswirth, S. Bolognani, G. Hug, and F. Dörfler, “Stability of dynamic feedback optimization with applications to power systems,” in *2018 56th Annual Allerton Conference on Communication, Control, and Computing (Allerton)*, 2018, pp. 136–143. DOI: 10.1109/ALLERTON.2018.8635640.
- [26] G. Belgioioso, D. Liao-McPherson, M. H. de Badyn, S. Bolognani, J. Lygeros, and F. Dörfler, “Sampled-data online feedback equilibrium seeking: Stability and tracking,” in *2021 60th IEEE Conference on Decision and Control (CDC)*, 2021, pp. 2702–2708. DOI: 10.1109/CDC45484.2021.9683614.
- [27] V. Häberle, A. Hauswirth, L. Ortmann, S. Bolognani, and F. Dörfler, “Non-convex feedback optimization with input and output constraints,” *IEEE Control Systems Letters*, vol. 5, no. 1, pp. 343–348, 2021. DOI: 10.1109/LCSYS.2020.3002152.
- [28] A. Hauswirth, S. Bolognani, G. Hug, and F. Dörfler, “Timescale separation in autonomous optimization,” *IEEE Transactions on Automatic Control*, vol. 66, no. 2, pp. 611–624, 2021. DOI: 10.1109/TAC.2020.2989274.
- [29] —, “Optimization algorithms as robust feedback controllers,” *arXiv:2103.11329*, 2021.
- [30] L. S. P. Lawrence, J. W. Simpson-Porco, and E. Mallada, “Linear-convex optimal steady-state control,” *IEEE Transactions on Automatic Control*, vol. 66, no. 11, pp. 5377–5384, 2021. DOI: 10.1109/TAC.2020.3044275.
- [31] S. Boyd and L. Vandenberghe, *Convex Optimization*. Cambridge University Press, 2004. DOI: 10.1017/CB09780511804441.
- [32] R. A. Horn and C. R. Johnson, *Matrix analysis*. Cambridge university press, 2012.
- [33] J. B. Carrell, “Groups, matrices, and vector spaces,” *A group theoretic approach to linear algebra*. Springer, New York, 2017.
- [34] H. Khalil, *Nonlinear Systems*, ser. Pearson Education. Prentice Hall, 2002, ISBN: 9780130673893. [Online]. Available: [https://books.google.com.lb/books?id=t%5C\\_d1QgAACAAJ](https://books.google.com.lb/books?id=t%5C_d1QgAACAAJ).
- [35] F. Zhang, *The Schur complement and its applications*. Springer Science & Business Media, 2006, vol. 4.
- [36] C. Desoer and E. Kuh, *Basic Circuit Theory*, ser. Electronic engineering systems series. McGraw-Hill, 1969, ISBN: 9780070851832. [Online]. Available: <https://books.google.com.lb/books?id=5J5TAAAAMAAJ>.
- [37] A. Sarlette, J. Dai, Y. Phulpin, and D. Ernst, “Cooperative frequency control with a multi-terminal high-voltage dc network,” *Automatica*, vol. 48, no. 12, pp. 3128–3134, 2012, ISSN: 0005-1098. DOI: <https://doi.org/10.1016/j.automatica.2012.08.017>. [Online]. Available: <https://www.sciencedirect.com/science/article/pii/S0005109812004189>.

- [38] J. Dai, Y. Phulpin, A. Sarlette, and D. Ernst, “Voltage control in an hvdc system to share primary frequency reserves between non-synchronous areas,” Aug. 2011.
- [39] K. Akbari-Moornani, “Model-predictive control of hvdc grid,” Ph.D. dissertation, University of Toronto (Canada), 2020.
- [40] R. Wachal, A. Jindal, S. Denetiere, *et al.*, *Guide for the development of models for hvdc converters in a hvdc grid*, Dec. 2014.
- [41] L. Lawrence, *The optimal steady-state control problem*, 2019.